variant has also been reported to cause a reduction in immunogenicity and allergenicity [21].

Domains I, II, and III contain one, three, and one N-glycosylation sites, respectively [7]. The possible relation between the carbohydrate chain in domain III and allergenicity is interesting. One report suggested that this carbohydrate chain may play an important role in allergenic determinants against human IgE antibody [13], and another report suggested that the carbohydrate chains of OVM may protect against peptic hydrolysis [22]. However, the carbohydrate moieties have been shown to have only a minor effect on allergenicity [23]. As shown in figure 2, intact OVM, FR 1, and FR 2 fragments were detected using PAS staining, suggesting the presence of carbohydrate chains, but FR 4 was not stained with the PAS reagent, despite being clearly detected with CBB. Therefore, FR 4 might contain little or no carbohydrate chains. Since FR 4 seems to maintain its allergenic potential, as described above, the absence of the carbohydrate chains in FR 4 suggests that they are not necessary for OVM allergenicity. Since the minimum peptide size capable of eliciting significant clinical symptoms of allergic reactions is thought to be 3.1 kDa [24], FR 4 may be able to trigger mast cell activation and elicit clinical symptoms.

In this report, the SGF-digestion kinetic pattern of OVM was investigated in detail, and the partial sequences of the fragments in the 4 fractions separated by SDS-PAGE were determined. Furthermore, the reactivity of the fragments with a number of serum samples from patients with egg white allergies was detected using Western blotting. The four fractions were separated according to their molecular weight and consisted of more than one fragment, as determined by N-terminal analysis. The identified sequences that started at Asn-104 and Val-134 in FR 3, as determined using LC/MS/MS (table 2), coincided with the 3-2 and 3-3 fragments in the N-terminal analysis (table 1), and the sequence that started at Asn-104 in FR 4 coincided with fragment 4-2. Moreover, the LC/MS/MS analysis indicated that FR 3 and FR 4 contained other parts of domain II and the C-terminal sequence N165–C185, which are thought to be minor components of these fractions. The combination of SGF digestion and patient IgE may provide useful information for the diagnosis and prediction of potential OVM allergenicity.

## Acknowledgement

This study was supported by a grant from the Ministry of Health, Labor and Welfare, and the Cooperative System for Supporting Priority Research of Japan Science and Technology Agency.

## References

1 Sampson HA, McCaskill CC: Food hypersensitivity and atopic dermatitis: Evaluation of 113 patients. J Pediatr 1985;107:669–675.
2 Bock SA, Sampson HA, Atkins FM, Zeiger RS, Lehrer S, Sachs M, Bush RK, Metcalfe DD: Double-blind, placebo-controlled food challenge (DBPCFC) as an office procedure: A manual. J Allergy Clin Immunol 1988;82:986–997.
3 Bock SA, Atkins FM: Patterns of food hypersensitivity during sixteen years of double-blind, placebo-controlled food challenges. J Pediatr 1990;117:561–567.
4 Boyano-Martinez T, Garcia-Ara C, Diaz-Pena JM, Martin-Esteban M: Prediction of tolerance on the basis of quantification of egg white-specific IgE antibodies in children with egg allergy. J Allergy Clin Immunol 2002;110:304–309.
5 Kotaniemi-Syrjanen A, Reijonen TM, Romppanen J, Korhonen K, Savolainen K, Korppi M: Allergen-specific immunoglobulin E antibodies in wheezing infants: The risk for asthma in later childhood. Pediatrics 2003;111:e255–e261.
6 Li-Chan E, Nakai S: Biochemical basis for the properties of egg white. Crit Rev Poultry Biol 1989;2:21–58.
7 Kato I, Schrode J, William J. Kohr WJ, Laskowski M Jr: Chicken ovomucoid: Determination of its amino acid sequence, determination of the trypsin reactive site, and preparation of all three of its domains. Biochemistry 1987;26:193–201.
8 Matsuda T, Watanabe K, Nakamura R: Immunochemical and physical properties of peptic-digested ovomucoid. J Agric Food Chem 1983;31:942–946.
9 Honma K, Aoyagi M, Saito K, Nishimuta T, Sugimoto K, Tsunoo H, Niimi H, Kohno Y: Antigenic determinants on ovalbumin and ovomucoid: Comparison of the specificity of IgG and IgE antibodies. Arerugi 1991;40:1167–1175.
10 Takagi K, Teshima R, Okunuki H, Sawada J: Comparative study of in vitro digestibility of food proteins and effect of preheating on the digestion. Biol Pharm Bull 2003;26:969–973.
11 Fu TJ, Abbott UR, Hatzos C: Digestibility of food allergens and nonallergenic proteins in simulated gastric fluid and simulated intestinal fluid-a comparative study. J Agric Food Chem 2002;50:7154–7160.
12 Zhang JW, Mine Y: Characterization of IgE and IgG epitopes on ovomucoid using egg-white-allergic patients' sera. Biochem Biophys Res Commun 1998;253:124–127.
13 Matsuda T, Nakamura R, Nakashima I, Hasegawa Y, Shimokata K: Human IgE antibody to the carbohydrate-containing third domain of chicken ovomucoid. Biochem Biophys Res Commun 1985;129:505–510.
14 Thomas K, Aalbers M, Bannon GA, Bartels M, Dearman RJ, Esdaile DJ, Fu TJ, Glatt CM, Hadfield N, Hatzos C, Hefle SL, Heylings JR, Goodman RE, Henry B, Herouet C, Holsapple M, Ladics GS, Landry TD, MacIntosh SC, Rice EA, Privalle LS, Steiner HY, Teshima R, Van Ree R, Woolhiser M, Zawodny J: A multilaboratory evaluation of a common in vitro pepsin digestion assay protocol used in assessing the safety of novel proteins. Regul Toxicol Pharmacol 2004;39:87–98.

15 Kovacs-Nolan J, Zhang JW, Hayakawa S, Mine Y: Immunochemical and structural analysis of pepsin-digested egg white ovomucoid. J Agric Food Chem 2000;48:6261–6266.
16 Besler M, Petersen A, Steinhart H, Paschke A: Identification of IgE-Binding Peptides Derived from Chemical and Enzymatic Cleavage of Ovomucoid (Gal d 1). Internet Symposium on Food Allergens 1999;1:1–12. http://www.food-allergens.de
17 Urisu A, Yamada K, Tokuda R, Ando H, Wada E, Kondo Y, Morita Y: Clinical significance of IgE-binding activity to enzymatic digests of ovomucoid in the diagnosis and the prediction of the outgrowing of egg white hypersensitivity. Int Arch Allergy Immunol 1999; 120:192–198.
18 Zacharius RM, Zell TE, Morrison JH, Woodlock JJ: Glycoprotein staining following electrophoresis on acrylamide gels. Anal Biochem 1969;30:148–152.
19 Mine Y, Zhang JW: Identification and fine mapping of IgG and IgE epitopes in ovomucoid. Biochem Biophys Res Commun 2002; 292:1070–1074.
20 Beyer K, Ellman-Grunther L, Jarvinen KM, Wood RA, Hourihane J, Sampson HA: Measurement of peptide-specific IgE as an additional tool in identifying patients with clinical reactivity to peanuts. J Allergy Clin Immunol 2003;112:202–207.
21 Mine Y, Sasaki E, Zhang JW: Reduction of antigenicity and allergenicity of genetically modified egg white allergen, ovomucoid third domain. Biochem Biophys Res Commun 2003; 302:133–137.
22 Matsuda T, Gu J, Tsuruta K, Nakamura R: Immunoreactive glycopeptides separated from peptic hydrolysate of chicken egg white ovomucoid. J Food Sci 1985;50:592–594.
23 Cooke SK, Sampson HA: Allergenic properties of ovomucoid in man. J Immunol 1997;159: 2026–2032.
24 Kane PM, Holowka D, Baird B: Cross-linking of IgE receptor complexes by rigid bivalent antigens greater than 200 Å in length triggers cellular degranulation. J Cell Biol 1988;107: 969–980.

RAPID COMMUNICATIONS IN MASS SPECTROMETRY
*Rapid Commun. Mass Spectrom.* 2004; 18: 1156–1160
Published online in Wiley InterScience (www.interscience.wiley.com). DOI: 10.1002/rcm.1465

# Improved sensitivity for insulin in matrix-assisted laser desorption/ionization time-of-flight mass spectrometry by premixing α-cyano-4-hydroxycinnamic acid matrix with transferrin

**Tetsu Kobayashi*, Hiroshi Kawai, Takuo Suzuki, Toru Kawanishi and Takao Hayakawa**
Division of Biological Chemistry and Biologicals, National Institute of Health Sciences, 1-18-1 Kamiyoga, Setagaya-ku, Tokyo 158-8501, Japan

Received 27 February 2004; Revised 25 March 2004; Accepted 25 March 2004

**This report describes an enhancement of the signal intensities of proteins and peptides in matrix-assisted laser desorption/ionization time-of-flight mass spectrometry (MALDI-TOFMS). When α-cyano-4-hydroxycinnamic acid (CHCA) premixed with human transferrin (Tf) was used as a matrix, the signal intensity of insulin was amplified to more than ten times that of the respective control in CHCA without Tf. The detection limit of insulin was 0.39 fmol on-probe in the presence of Tf, while it was 6.3 fmol in the absence of Tf. The signal intensity of insulin was also enhanced when the CHCA matrix was premixed with proteins other than Tf (80 kDa), such as horse ferritin (20 kDa), bovine serum albumin (BSA, 66 kDa), or human immunoglobulin G (150 kDa). The optimum spectrum of insulin was obtained when the added amount of protein was in the range 0.26–0.62 pmol, regardless of the molecular weight of the added protein. Tf and BSA outperformed the other tested proteins, as determined by improvements in the resulting spectra. When the mass spectra of several peptides and proteins were recorded in the presence of Tf or BSA, the signal intensities of large peptides such as glucagon were enhanced, though those of smaller peptides were not enhanced. In addition, the signal enhancement achieved with Tf and BSA was more pronounced for the proteins, including cytochrome C, than for the large peptides. This enhancement effect could be applied to improve the sensitivity of MALDI-TOFMS to large peptides and proteins. Copyright © 2004 John Wiley & Sons, Ltd.**

Matrix-assisted laser desorption/ionization time-of-flight mass spectrometry (MALDI-TOFMS) and electrospray ionization mass spectrometry have been widely used in studies of protein chemistry, including proteomics studies aimed at sequence identification or quantitative analyses following enzymatic digestion by isotope-coded affinity tags and other tagging systems.[1–8] In particular, MALDI-TOFMS has been used for the qualitative and quantitative analysis of intact proteins.[9–11] When the MALDI technique was first introduced as an ionization method for proteins, a mixture of fine metal powder and glycerol, or nicotinic acid, was used as the matrix.[12,13] Progress has been made with other matrix materials such as sinapinic acid, 2,5-dihydroxybenzoic acid (DHB), and α-cyano 4-hydroxycinnamic acid (CHCA), which have some desirable properties such as less intense adduct peaks and a relative insensitivity to contamination.[14–16] With the MALDI approach, analyte proteins are dispersed on a surface in a thin layer of matrix. The energy of an incident pulse of laser photons is absorbed by the matrix to form a jet of matrix vapor that lifts the analyte proteins from the surface and transforms some of them into ions.[13]

However, the mechanisms by which laser light irradiation is able to generate macromolecular ions have not been fully verified to date. It has been reported that the ionization of macromolecules by the MALDI process is affected by several factors. For example, peptide signal intensity was increased by the use of acetone as the solvent for CHCA matrix instead of employing the commonly used solvent, a mixture of acetonitrile and aqueous 0.1% trifluoroacetic acid (TFA).[17] The signal-to-noise (S/N) ratios for macromolecules are low in DHB matrix, but the addition of suitable additives (fructose, glucose, fucose, or 2-hydroxy-5-methoxybenzoic acid) to the DHB matrix improved its performance in the high molecular mass range.[18–21] In the CHCA and sinapinic acid matrices, the detection of higher molecular weight proteins was improved by using polytetrafluoroethylene (Teflon) as sample support.[22,23]

Recently, we investigated a method of identifying and quantifying proteins in blood using mass spectrometry. During the present study, we discovered that the signal intensity of human insulin was augmented more than 10-fold when transferrin (Tf) was mixed with the CHCA matrix

**Correspondence to*: T. Kobayashi, Division of Biological Chemistry and Biologicals, National Institute of Health Sciences, 1-18-1 Kamiyoga, Setagaya-ku, Tokyo 158-8501, Japan.
E-mail: kobayash@nihs.go.jp
Contract/grant sponsor: Ministry of Health, Labor and Welfare, Japan.

solution used for MALDI-TOFMS. This phenomenon was not specific to either insulin or Tf, which suggested that such enhancements could be used more generally to improve the sensitivity of protein analysis with MALDI-TOFMS.

## EXPERIMENTAL

### Materials

Human atrial natriuretic peptide (hANP), glucagon, insulin, insulin-like growth factor-1 (IGF-1), transferrin (Tf), bovine serum albumin (BSA), horse spleen ferritin (106 mg/mL in 0.15 M NaCl), and ProteoMass Peptide & Protein, were purchased from Sigma (St. Louis, MO, USA). Human immunoglobulin G (IgG, 11.3 mg/mL in 0.01 M sodium phosphate, 0.5 M NaCl, pH 7.6) was obtained from Wako Pure Chemical Industries Ltd. (Tokyo, Japan). Human insulin, IGF-1, glucagon, and hANP stock solutions were prepared at concentrations of 100 pmol/μL by dissolving them in 0.1% TFA. Tf and BSA stock solutions were prepared at concentrations of 10 mg/mL by dissolving the materials in Millipore deionized water. ProteoMass Peptide & Protein stock solutions, which include bradykinin fragment 1-7, human angiotensin II, synthetic peptide $P_{14}R$, human ACTH fragment 18-39, bovine insulin oxidized B chain, bovine insulin, equine cytochrome C, equine apomyoglobin, rabbit aldolase, and BSA, were prepared at concentrations of 100 pmol/μL each, according to the manufacturer's instructions.

### Sample application and data acquisition

The Tf-mixed CHCA was a 5:1 mixture of the CHCA solution (10 mg/mL in 50% acetonitrile in 0.1% aqueous TFA) and Tf solution (0.10 μg/μL; the final concentration was approximately 8.3 ng/μL), corresponding to 0.21 pmol Tf on each well of the target plate, if not otherwise noted. The control CHCA was a mixture of the CHCA solution and deionized water (5:1). A portion of each sample solution was immediately mixed with an equal volume of the matrix solution with or without Tf, and an aliquot of 2 μL (corresponding to 1 μL of sample solution) was applied to a stainless steel target plate. Mass spectrometric analyses were performed using an AB4700 proteomics analyzer (Applied Biosystems, Foster, CA, USA). The operating conditions were as follows: Nd:YAG laser (355 nm), linear mode, and detection of positive ions. The spectra were generated by signal averaging 50 laser shots into a single spectrum. The signal intensity was obtained after performing background correction and noise reduction using the Data Processor software (Applied Biosystems). This software was also used to determine the detection limit.

To confirm whether or not the matrix solution was at an optimum composition, serially diluted CHCA, DHB, or sinapinic acid solutions (from 10 to 0.078 mg/mL in 50% acetonitrile, 50% 0.1% TFA) were added to the insulin solution (100 fmol/μL). The most intense signal was obtained when 10 mg/mL CHCA was added to the insulin solution.

## RESULTS AND DISCUSSION

Human insulin solution (6.3 fmol/μL) was mixed with an equal volume of Tf-mixed CHCA or control CHCA. When

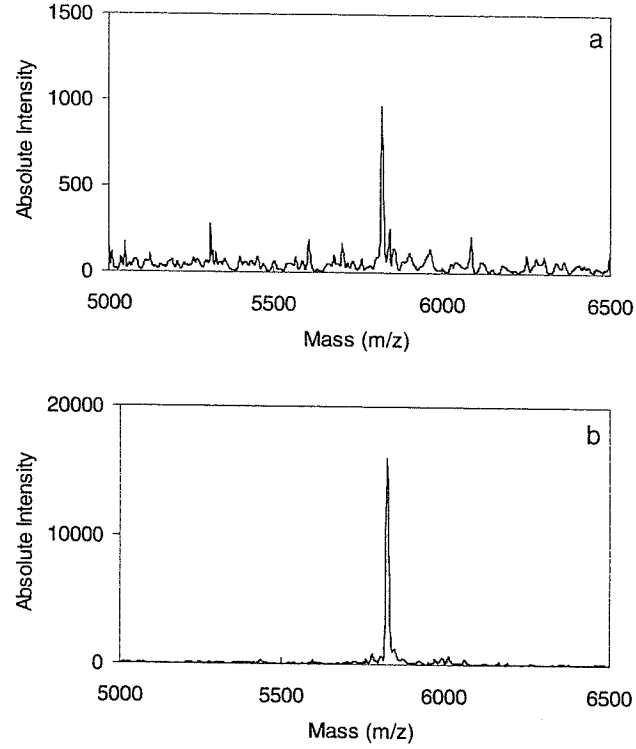


**Figure 1.** MALDI mass spectra of human insulin. The insulin solution (6.3 fmol/μL) and matrix solution were mixed together in equal volumes; 2 μL of the resulting mixture were applied to a target plate, allowed to dry, and analyzed by MALDI-TOFMS (see Experimental). The matrix solution was a 5:1 mixture of CHCA solution (10 mg/mL in 50% acetonitrile in 0.1% aqueous TFA) with deionized water or Tf solution (0.10 μg/μL). (a) Control CHCA used as matrix. (b) Tf-mixed CHCA used as matrix.

the Tf-mixed CHCA was used as matrix, the signal intensity of insulin in the MALDI-TOFMS detection system was amplified more than 10-fold relative to that achieved with the control CHCA (Fig. 1). To assess the sensitivity of insulin detection, the matrix solution was added to serially diluted insulin solutions (from 100 to 0.20 fmol/μL in deionized water), and samples were then spotted on a target plate. The detection limit of insulin was 0.39 fmol on the target plate in a Tf-mixed CHCA matrix under the present experimental conditions, whereas this limit was 6.3 fmol in the case of CHCA without Tf (Fig. 2).

To obtain the optimum concentration of Tf for the enhancement of insulin measurement sensitivity, the CHCA solution was mixed with serially diluted Tf solutions (from 1.0 μg/μL to 7.8 ng/μL) before addition to the insulin solution (100 fmol/μL). The signal intensity increased in a Tf-concentration-dependent manner (Fig. 3(a)). However, the S/N ratio decreased when the Tf concentration was more than 125 ng/μL (Fig. 3(b)), though it should be noted that the S/N value was still higher than the corresponding control value, i.e., 15 ± 7. A signal for 0.39 fmol/μL insulin was detected in the CHCA solution mixed with 0.1 μg/μL Tf (Fig. 2), whereas the signal for 1.6 fmol/μL insulin was not detected in the CHCA solution mixed with 1.0 μg/μL Tf (data not shown). These results suggest that the detection limit was also decreased in the presence of a high concentration of Tf.

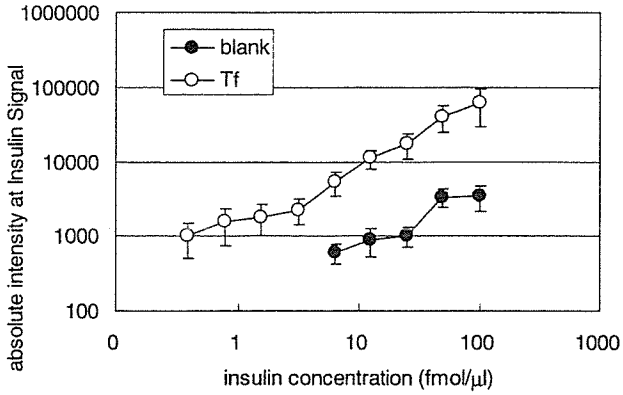


**Figure 2.** Dependence of insulin signals on insulin concentration. Sequentially diluted human insulin solution (100 to 0.20 fmol/μL in deionized water) and matrix solution were mixed in equal volumes. The matrix solution was a 5:1 mixture of the CHCA solution with either deionized water or Tf solution (0.10 μg/μL). The absolute intensity of the insulin signal obtained from Tf-mixed CHCA (open circles) is compared with that obtained for the control CHCA (closed circles). Each point represents the mean ± S.E. of four tests.

It is known that an excess amount of protein components can strongly influence the behavior of the MALDI process, resulting in partial or complete ion signal suppression.[24] In addition, the optimum mass ratio between the analyte and matrix for MALDI analysis has been demonstrated empirically.[15] When the CHCA was mixed with 1.0 μg/μL Tf, the excess amount of Tf might have suppressed the signal intensity of insulin as well. However, if that amount is appropriate, Tf appears somehow capable of enhancing the signal.

To determine whether or not the enhancement of the insulin MALDI-TOFMS signal intensity was specific to Tf, the CHCA solution was mixed with serially diluted solutions of several peptides and proteins before its addition to the insulin solution. The insulin signal intensity was also enhanced in the presence of ferritin (20 kDa), BSA (66 kDa), or IgG (150 kDa) (Fig. 4(a)). However, this was not found to occur in a simple concentration-dependent manner in the case of either ferritin or IgG; furthermore, when the CHCA solution was mixed with more than 2.0 μg/μL of these protein solutions, no insulin signal was detected. The enhancement of the insulin signal intensity was relatively small in the presence of peptides such as hANP (3.1 kDa) and glucagon (3.4 kDa). In addition, when the CHCA solution was mixed with more than 77 ng/μL of hANP or 87 ng/μL of glucagon, no insulin signal was detected. Among the tested peptides and proteins, the insulin signal intensity was enhanced most effectively in the presence of Tf (80 kDa) or BSA. Therefore, it is probable that this type of enhancement requires an added protein of moderate molecular weight, namely 66–80 kDa.

With regard to the results for the serial dilutions of the added peptides and proteins, the highest S/N values were obtained at 4.8 ng/μL hANP, 5.4 ng/μL glucagon, 66 ng/μL ferritin, 0.13 μg/μL BSA, 0.13 μg/μL Tf, or 0.57 μg/μL

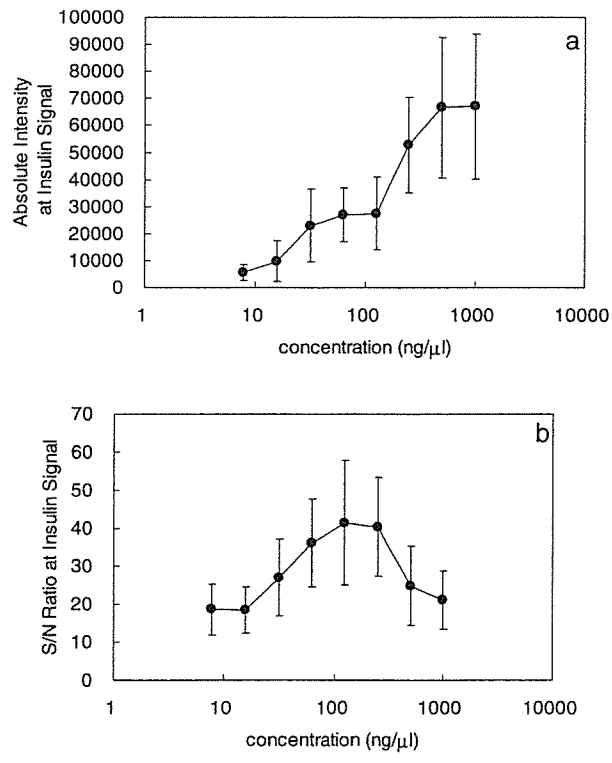


**Figure 3.** Dependence of insulin signal on Tf concentration. Serially diluted Tf solution was added to five volumes of the CHCA solution before mixing the resulting solution with an equal volume of human insulin (100 fmol/μL): (a) absolute intensity (arbitrary units) and (b) S/N ratio of the insulin signal in the MALDI analysis. Each point represents the mean ± S.E. of four tests.

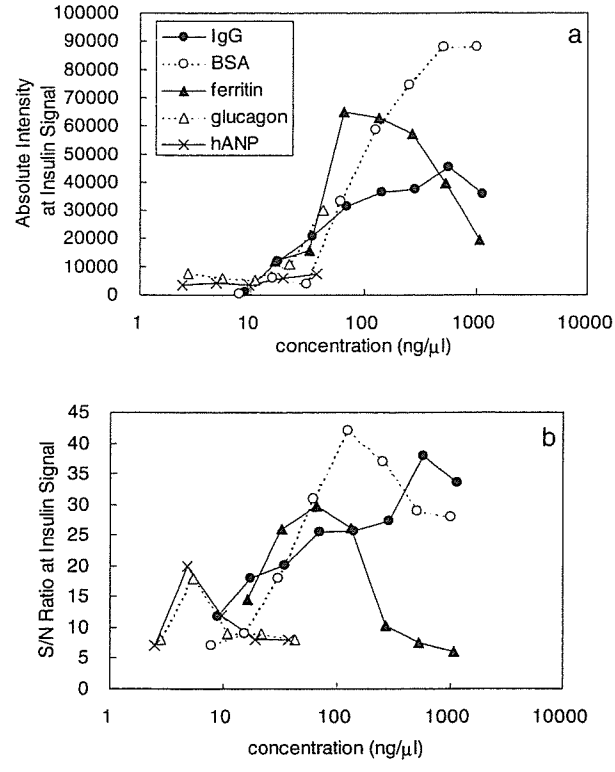


**Figure 4.** Dependence of insulin signal on concentrations of various added proteins. Serially diluted IgG, BSA, ferritin, glucagon, or hANP solution was added to the CHCA solution before the solution was mixed with the human insulin solution (100 fmol/μL): (a) absolute intensity (units) and (b) S/N ratio of the insulin signal. Each point represents the average of duplicate samples.

IgG (Figs. 3(b) and 4(b)), which correspond to 0.26 pmol, 0.26 pmol, 0.50 pmol, 0.32 pmol, 0.26 pmol, and 0.62 pmol, respectively, in each well. Thus, the optimum molar concentrations occurred in the same scale order, although the optimum mass concentrations of polypeptides required to enhance the signal differed markedly between the proteins and small peptides. In addition, the molar concentrations of excess peptides or proteins required to suppress the insulin signal were also found to exhibit the same scale in the same order. The ionization of insulin appeared to depend on the molar concentration of the peptide or protein which was mixed with the CHCA matrix solution.

To examine whether or not the signal enhancement was specific to human insulin, the CHCA solution premixed with Tf or BSA (0.10 μg/μL) was added to a solution of peptides and proteins, which included hANP, glucagon, human insulin, IGF-I, and ProteoMass Peptide & Protein at concentrations of 50 fmol/μL each. The signal intensities of [angiotensin II]$^+$ (1046 Da), [synthetic peptide $P_{14}R$]$^+$ (1534 Da), and [ACTH fragment]$^+$ (2465 Da) were either not enhanced or were reduced in the matrix premixed with Tf or BSA (Table 1). However, the signal intensities of [hANP]$^+$ (3080 Da), [glucagon]$^+$ (3483 Da), [insulin B chain]$^+$ (3494 Da), and [bovine insulin]$^+$ (5730 Da) were enhanced as well as that of [human insulin]$^+$ (5808 Da) (Table 1, Fig. 5). The signal intensities of [IGF-I]$^+$ (7649 Da), [cytochrome C]$^+$ (12 362 Da), and [cytochrome C]$^{2+}$ were enhanced more than that of human insulin in the presence of Tf or BSA. In addition, the signals of [apomyoglobin]$^+$ (16 952 Da) and [apomyoglobin]$^{2+}$ were clearly observed in the presence of Tf or BSA, although their signals were not detected in the control matrix. In this latter case, the signal of [apomyoglobin]$^+$ overlapped with that of BSA, but not of Tf; therefore, it was more advantageous to use Tf than BSA for detecting this signal. Since BSA was included in the ProteoMass Peptide & Protein solution, the signals of [BSA]$^+$ (66 430 Da), [BSA]$^{2+}$, [BSA]$^{3+}$, and [BSA]$^{4+}$ were also detected in the presence of Tf (Table 1, Fig. 5(b)).

The results reported above demonstrate that the enhancement of the signal intensity achieved with the use of Tf and BSA was observed for both peptides and proteins, and this effect was not specific to human insulin. The degree of enhancement was dependent on the molecular weights of the peptides and proteins, and no such enhancement was observed in the case of small peptides; in this regard a dividing line appeared to exist between [ACTH fragment]$^+$ (2465 Da) and [hANP]$^+$ (3080 Da).

The mechanism by which signal intensity enhancement was achieved with the use of peptides and proteins mixed with the matrix solution remains unclear. However, when super DHB (a co-matrix of DHB and 2-hydroxy-5-methoxybenzoic acid) was used as the matrix, ion yields and S/N ratio improved, especially for the high-mass range.[20] It has been suggested that this signal enhancement was caused by a disorder in the DHB lattice, allowing 'softer' desorption. This type of signal enhancement has also been observed in the case of substance P in CHCA after fast evaporation of an acetone solvent, which resulted in the more homogeneous distribution of matrix and analytes.[18] In addition, better mass resolution has been observed in the spectra of cytochrome C in a CHCA matrix desorbed from polyethylene and polypropylene membranes than has been observed with a CHCA matrix desorbed from stainless steel; it was thus suggested that such improved resolution might be due at least in part to the formation of relatively small matrix crystals within the membrane lattice structure.[25] In the present study, Tf and other proteins might have led to a similar disorganization in the CHCA lattice, resulting in the homogeneous distribution of insulin in the CHCA. However, the mechanism may differ from that suggested here, since the disorder in the CHCA lattice cannot reasonably account for why both Tf and BSA were able to enhance the insulin signal more effectively than either hANP or glucagon. As the next step, we are now planning to compare the crystals of the additive macromolecules plus matrix with those of the control matrix, using microscopic examination, to help elucidate the enhancement mechanism. We also intend to investigate whether the enhancement effect is observed in matrices other than CHCA. If crystallization is important,

**Table 1.** Signal intensities for proteins and peptides obtained using a matrix premixed with deionized water or with solutions of Tf or BSA

| | Water | Tf | BSA |
|---|---|---|---|
| [Angiotensin II]$^+$ | 27 834 ± 10 757 | 17 057 ± 5021 | 19 755 ± 11 237 |
| [P14R]$^+$ | 41 689 ± 15 289 | 30 675 ± 8588 | 29 237 ± 13 330 |
| [ACTH 18–39]$^+$ | 4371 ± 1586 | 3801 ± 2246 | 5458 ± 3826 |
| [hNAP]$^+$ | 5158 ± 1323 | 6889 ± 2879 | 9523 ± 6384 |
| [human glucagon]$^+$ | 435 ± 183 | 674 ± 324 | 978 ± 566 |
| [insulin B chain]$^+$ | 367 ± 257 | 997 ± 251 | 715 ± 479 |
| [bovine insulin]$^+$ | 639 ± 100 | 6266 ± 2736 | 7498 ± 5331 |
| [human insulin]$^+$ | 1267 ± 130 | 13 321 ± 5057 | 12 982 ± 6863 |
| [equine cytochrome C]$^{2+}$ | 166 ± 83 | 5668 ± 1975 | 3460 ± 1442 |
| [human IGF-I]$^+$ | 459 ± 81 | 7667 ± 1808 | 6263 ± 2872 |
| [equine apomyoglobin]$^{2+}$ | nd | 2249 ± 994 | 2217 ± 1087 |
| [equine cytochrome C]$^+$ | 114 ± 43 | 7629 ± 1804 | 4006 ± 1981 |
| [BSA]$^{4+}$ | nd | 52 ± 14 | 2459 ± 604 |
| [equine apomyoglobin]$^+$ | nd | 1347 ± 700 | 2090 ± 1316 |
| [BSA]$^{3+}$ | nd | 155 ± 13 | 3721 ± 1426 |
| [BSA]$^{2+}$ | nd | 114 ± 27 | 3624 ± 1681 |
| [BSA]$^+$ | nd | 25 ± 8 | 634 ± 433 |

Each entry is the average of the most intense signals from four samples. nd: no signal was detected.

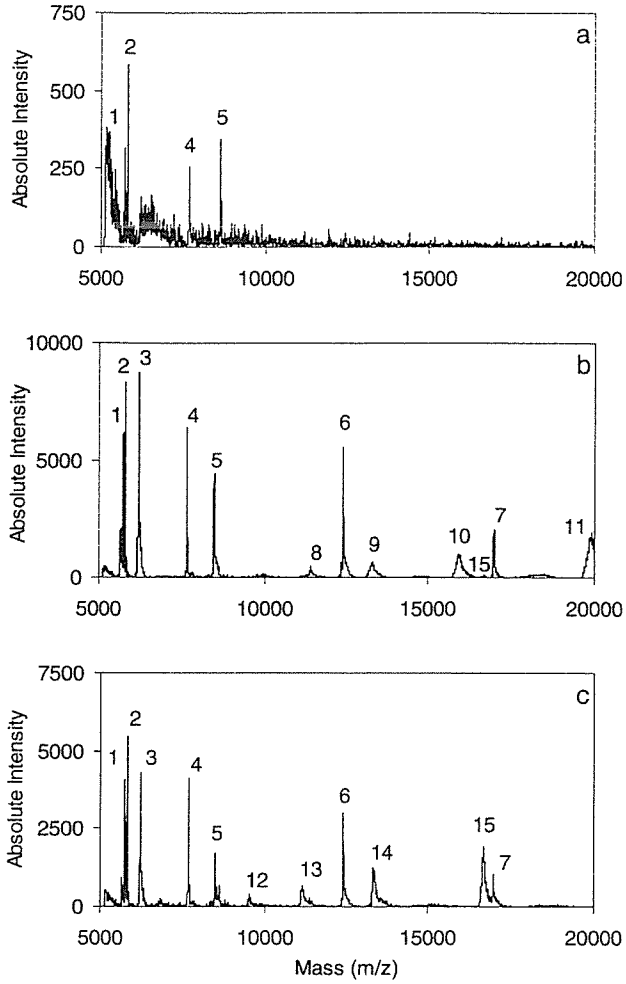


**Figure 5.** MALDI mass spectra of a mixture of peptides and proteins. The mixture of peptides and proteins (50 fmol/μL each) and the matrix solution were mixed together in equal volumes. The matrix solution was a 5:1 mixture of the CHCA solution with (a) deionized water; (b) Tf solution (0.10 μg/μL); and (c) BSA solution (0.10 μg/μL). Signal 1, [bovine insulin]$^{+}$ (5730 Da); 2, [human insulin]$^{+}$ (5808 Da); 3, [cytochrome C]$^{2+}$; 4, [IGF-I]$^{+}$ (7649 Da); 5, [apomyoglobin]$^{2+}$; 6, [cytochrome C]$^{+}$ (12 362 Da); 7, [apomyoglobin]$^{+}$ (16 952 Da); 8, [Tf]$^{7+}$; 9, [Tf]$^{6+}$; 10, [Tf]$^{5+}$; 11, [Tf]$^{4+}$; 12, [BSA]$^{7+}$; 13, [BSA]$^{6+}$; 14, [BSA]$^{5+}$; and 15, [BSA]$^{4+}$.

the effect should not be observed when using liquid matrices.[26,27]

The present results suggest that the enhancement brought about by either Tf or BSA could be applicable to the improvement of sensitivity in the detection of proteins by MALDI-TOFMS in general. However, when Tf or BSA was used as an enhancer in a MALDI-TOFMS system, signals from Tf and BSA were also detected, which sometimes interfered with the analysis of the target proteins. Therefore, neither Tf nor BSA appears to be the best possible enhancer. Further studies are currently underway in order to discover the best macromolecule as an enhancer.

## CONCLUSIONS

We have demonstrated that the signal intensities of insulin and of several peptides and proteins were enhanced in CHCA premixed with Tf or other peptides or proteins. The characteristics of this type of enhancement are as follows: (1) Tf (80 kDa) and BSA (66 kDa) led to better signal enhancement than did small peptides and proteins (<20 kDa) or IgG (150 kDa); (2) the optimum S/N value was observed when the added amount of peptide or protein was within the range 0.26–0.62 pmol; and (3) the signals of peptides of high molecular weight (>3000 Da) were enhanced by the addition of Tf or BSA to CHCA, although the signals of small peptides (<2500 Da) were not enhanced. This type of enhancement may be useful for the improvement of protein analyses with MALDI-TOFMS.

## Acknowledgements

This study was supported in part by a research grant on Human Genome, Tissue Engineering Food Biotechnology from the Ministry of Health, Labor and Welfare, Japan.

## REFERENCES

1. Roberts GD, Johnson WP, Burman S, Anumula KR, Carr SA. *Anal. Chem.* 1995; **67**: 3613.
2. Gygi SP, Rist B, Gerber SA, Turecek F, Gelb MH, Aebersold R. *Nat. Biotechnol.* 1999; **17**: 994.
3. Münchbach M, Quadroni M, Miotto G, James P. *Anal. Chem.* 2000; **72**: 4047.
4. Yao X, Freas A, Ramirez J, Demirev PA, Fenselau C. *Anal. Chem.* 2001; **73**: 2836.
5. Cagney G, Emili A. *Nat. Biotechnol.* 2002; **20**: 163.
6. Vogt JA, Schroer K, Hözler K, Hunzinger C, Klemm M, Biefang-Arndt K, Schillo S, Cahill MA, Schlattenholz A, Matthies H, Stegmann W. *Rapid Commun. Mass Spectrom.* 2003; **17**: 1273.
7. Kuyama H, Watanabe M, Toda C, Ando E, Tanaka K, Nishimura O. *Rapid Commun. Mass Spectrom.* 2003; **17**: 1642.
8. Wu SL, Choudhary G, Ramström M, Bergquist J, Hancock WS. *J. Proteome Res.* 2003; **2**: 383.
9. Nakanishi T, Okamoto N, Tanaka K, Shimizu A. *Biol. Mass Spectrom.* 1994; **23**: 230.
10. Nelson RW, Krone JR, Bieber AL, Williams P. *Anal. Chem.* 1995; **67**: 1153.
11. Tubbs KA, Nedelkov D, Nelson RW. *Anal. Biochem.* 2001; **289**: 26.
12. Tanaka K, Waki H, Ido Y, Akita S, Yoshida Y, Yoshida T. *Rapid Commun. Mass Spectrom.* 1988; **2**: 151.
13. Karas M, Hillenkamp F. *Anal. Chem.* 1988; **60**: 2299.
14. Beavis RC, Chait BT. *Anal. Chem.* 1990; **62**: 1836.
15. Strupat K, Karas M, Hillenkamp F. *Int. J. Mass Spectrom. Ion Processes* 1991; **111**: 89.
16. Beavis RC, Chaudhary T, Chait BT. *Org. Mass Spectrom.* 1992; **27**: 156.
17. Vorm O, Roepstorff P, Mann M. *Anal. Chem.* 1994; **66**: 3281.
18. Köstler C, Castoro JA, Wilkins CL. *J. Am. Chem. Soc.* 1992; **114**: 7572.
19. Billeci TM, Stults JT. *Anal. Chem.* 1993; **65**: 1709.
20. Karas M, Ehring H, Nordhoff E, Stahl B, Strupat K, Hillenkamp F, Grehl M, Krebs B. *Org. Mass Spectrom.* 1993; **28**: 1476.
21. Tsarbopoulos A, Karas M, Strupat K, Pramanik BN, Nagabhushan TL, Hillenkamp F. *Anal. Chem.* 1994; **66**: 2062.
22. Yuan X, Desiderio DM. *J. Mass Spectrom.* 2002; **37**: 512.
23. Botting CH. *Rapid Commun. Mass Spectrom.* 2003; **17**: 598.
24. Nelson RW, McLean MA. *Anal. Chem.* 1994; **66**: 1408.
25. Worrall TA, Cotter RJ, Woods AS. *Anal. Chem.* 1998; **70**: 750.
26. Carda-Broch S, Berthod A, Armstrong DW. *Rapid Commun. Mass Spectrom.* 2003; **17**: 553.
27. Turney K, Harrison WW. *Rapid Commun. Mass Spectrom.* 2004; **18**: 629.

〔シンポジウム：Functional Glycomics ミニレビュー〕

# LC/MSを用いた糖鎖プロファイリングによるグライコーム解析

川崎ナナ・橋井則貴・伊藤さつき・日向昌司・川西 徹・早川堯夫


## SUMMARY

Liquid chromatography/mass spectrometry equipped with a graphitized carbon column is useful for the simultaneous analysis of oligosaccharides. By using capillary column and nanoelectrospray ion source, the method can be used for the oligosaccharide profiling of sub microgram quantities of glycoproteins. This oligosaccharide profiling is expected to be a powerful tool for the glycome analysis. We demonstrate a potential application of oligosaccharide profiling in glycomics with two examples, the structural analysis of *N*-linked oligosaccharides from a gel-separated glycoprotein, and the differential analysis of *N*-linked oligosaccharides in cells.


Key words: LC/MS, oligosaccharide profiling, 2-dimensional electrophoresis, glycomics.

## はじめに

糖タンパク質の糖鎖の構造や不均一性は，発生・加齢・疾病等に関連して変化することが知られている[1]．しかし，従来のプロテオミクス的アプローチ，すなわち，2次元電気泳動（2-DE）等でタンパク質発現量を比較し，差異の認められたタンパク質を質量分析法（MS）とデータベース検索により同定するという方法[2]では，糖鎖の変化によって引き起こされる生命現象を捉えることはできない．糖タンパク質の糖鎖部分が関係する様々な現象を解明するには，糖鎖の定性的・定量的解析に基づくグライコーム解析技術の開発が不可欠である．

MSと液体クロマトグラフィー（LC）をオンラインで結んだLC/MSは，分子量情報だけでなく，多くの異性体が存在する糖鎖の詳細な構造や不均一性に関する情報を提供してくれることから，今後，糖鎖生物学分野においても有力なツールとなることが期待されている．我々は，極性物質の吸着能が高く，エレクトロスプレーイオン化（ESI）に適した溶媒で糖鎖を分離・溶出できるグラファイトカーボンカラム（GCC）を用いることによって，高マンノース型，複合型，混成型糖鎖や，酸性糖鎖，中性糖鎖など様々な糖鎖を一度に分離・検出できる糖鎖プロファイリング法を開発した[3,4]．この糖鎖プロファイリング法は，グライコーム解析の様々なステップにおいても役立つと思われる．本稿では，グライコーム解析における糖鎖プロファイリングの可能性として，2-DEで分離されたゲル内糖タンパク質の糖鎖構造解析に応用した例と，細胞発現糖タンパク質の糖鎖の差異解析に応用した例を紹介する．

## I. ゲル内糖タンパク質の糖鎖構造解析

### 1. 糖鎖プロファイリング法の微量化

一般に2-DEとクマシーブルー（CBB）染色によって検出可能な糖タンパク質量は1 μg程度といわれているが，ゲルからの回収率や操作中の損失等を考慮に入れると，サブマイクログラムのタンパク質に由来する糖鎖を解析できる分析システムが必要となる．そこで，キャピラリーカラムとナノスプレーイオン源を用いて，糖鎖プロファイリングの微量化を検討した．

NS0細胞産生遺伝子組換え型ヒト肝細胞増殖因子（HGF）に*N*-グリコシダーゼF（PNGase F）を作用させて*N*結合糖鎖を切り出し，anomerの分離を避けるため$NaBH_4$で還元した．200 ngのHGFに由来する糖鎖をGCC-LC/MSを

---

Glycome analysis by oligosaccharide profiling using liquid chromatography/mass spectrometry.

Nana Kawasaki, Noritaka Hashii, Satsuki Itoh, Masashi Hyuga, Toru Kawanishi, Takao Hayakawa; 国立医薬品食品衛生研究所生物薬品部

Correspodence address: Nana Kawasaki; Division of Biological Chemistry and Biologicals, National Institute of Health Sciences, 1-18-1, Kamiyoga, Setagaya-ku, Tokyo 158-8501, Japan

第53回日本電気泳動学会シンポジウム

（受付2003年11月13日，受理2003年11月20日，刊行2004年3月15日）

用いて分析したところ，トータルイオンクロマトグラム（TIC）上に2つの大きなピークと，複数の小さいピークが確認された（Fig. 1A）．ピークAは，マススペクトル（Fig. 1B），及びプロダクトイオンスペクトル（Fig. 1C）から，*N*-グリコリルノイラミン酸（NeuGc）及びヘキソース（Hex）-Hexを部分構造とする複合型糖鎖であることが示唆された．他のピークについても同様に，NeuGc及びHex-Hex構造が存在することが推定された．そこで，Hex-Hex構造を確認するため，糖鎖をα-ガラクトシダーゼで消化し，再度LC/MSで分析を行ったところ，Fig. 1A上で検出されたピークが消失し，新たに複数のピークが出現することが確認された．これらのピークの分子量は，α-ガラクトシダーゼ消化前の糖鎖からGalが1または2分子消失した糖鎖の分子量に一致することから，HGFの非還元末端には1または2分子のGalがα結合していることが確認された[5]．NS0細胞産生糖タンパク質にはGalα1-3Galを含む糖鎖が結合していることが報告されており[6,7]，今回検出されたHex-HexもGalα1-3Gal結合であると推定された．これらのことから，ピークAの糖鎖構造はFig. 1C上図のように推定され，他のピークについても，NeuGc及びGalα1-3Gal結合を部分構造とする複合型糖鎖であると考えられた．

以上のように，キャピラリーカラムとナノスプレーイオン源を用いることによって，サブマイクログラムの糖タンパク質の糖鎖のプロファイリングが可能となった．また，LC/MS/MS，及びエキソグリコシダーゼ消化とLC/MSを組み合わせることによって，より詳細な構造情報が得られることが確認された．

## 2. ゲル内糖タンパク質の糖鎖構造解析

つぎに，GCC-LC/MSを用いた電気泳動ゲル内糖タンパク質の糖鎖のプロファイリングを検討した．2 μgのヒト黒色腫細胞産生ヒト組織プラスミノーゲンアクチベータ（tPA）をSDS-PAGEで展開し（Fig. 2A），ゲル内PNGase F消化により糖鎖を切り出した．$NaBH_4$還元糖鎖をLC/MSで分析したところFig. 2Bのような糖鎖プロファイルが得られ，ゲルから抽出されたtPAの糖鎖の分離パターンは，泳動前の分離パターンとほぼ同様であることが確認された．

以上のように，CBB染色される程度の糖タンパク質があれば，ゲル内タンパク質であっても，GCC-LC/MSによる糖鎖プロファイリングが可能であることが確認された．ゲル内タンパク質糖鎖の解析法として，2-aminobenzamide誘導体化後，イオン交換や順相LCで分離し，オフラインMALDI-TOFMSで解析する手法が報告されている[8]．我々は，GCC-LC/MSを用いた解析は誘導体化における糖鎖の分解が生じ

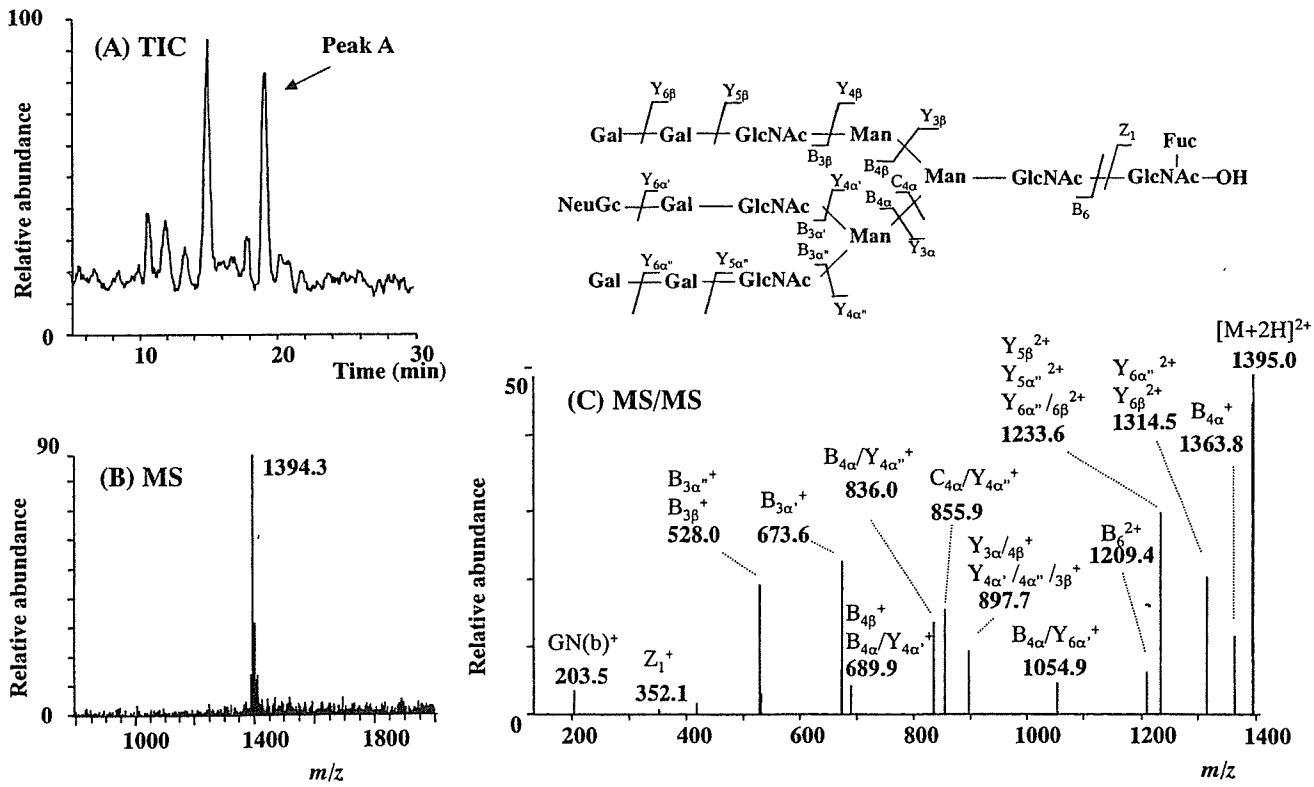


Fig. 1. (A) GCC-LC/MSによって得られたHGFの糖鎖プロファイル，(B) ピークAのマススペクトル，(C) ピークAのプロダクトイオンスペクトル及び推定構造

カラム，Hypercarb（0.2×150 mm）；流速，3 μl/min；溶離液，5 mM酢酸アンモニウム/$H_2O$-アセトニトリル；MS，TSQ-7000（Thermoelectron）

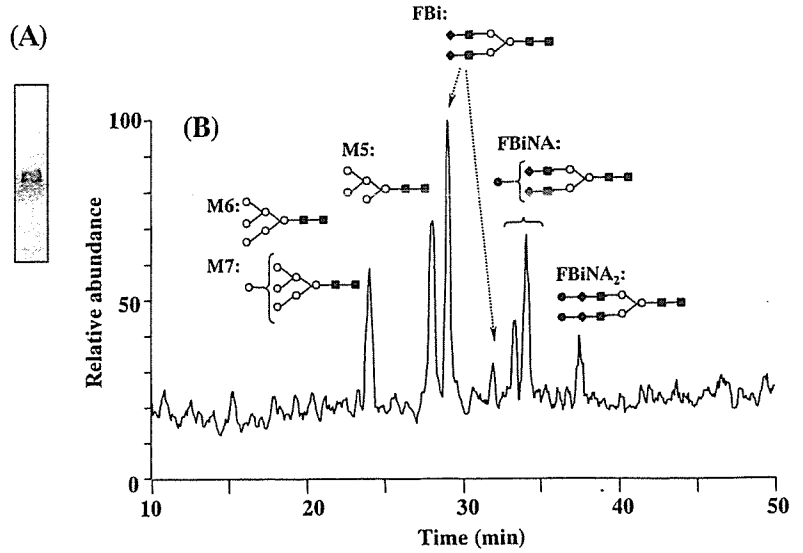


Fig. 2. (A) tPA (2 μg) の SDS-PAGE, (B) GCC-LC/MS によるゲル内 tPA 由来糖鎖のプロファイル

ないこと，1 回の LC で異性体を含む様々な糖鎖を分離できること，ESI を用いているのでシアル酸結合糖鎖や硫酸化糖鎖の解析にも応用できること，オンライン MS による簡便・迅速な分析が可能な上，マイナー成分の取りこぼしがないこと等の利点があると考えている．

## II. 細胞・組織発現糖タンパク質糖鎖の差異解析

### 1. 糖鎖の差異解析

疾患組織と健常組織に発現している糖タンパク質の糖鎖の分布を直接比較し，疾患関連糖鎖遺伝子や糖タンパク質を見つけ出すことができれば，新たな診断法の開発や糖鎖と疾患の関係の解明につながるものと期待される．そこで，GCC-LC/MS を用いて，簡単な操作と実行可能なサンプル量で，サンプル間の糖鎖の差異解析を行うことを検討した．モデルとして，糖鎖遺伝子導入によって糖鎖の構造と分布が変化していることが予想される細胞を用いた．*N*-アセチルグルコサミン転移酵素 III (GnT-III) は，複合型 2 本鎖糖鎖に bisecting GlcNAc を付加する糖転移酵素で，細胞接着や癌転移と関係があることが報告されている[9～11]．ここでは，GnT-III 遺伝子を導入した CHO 細胞を病態モデルとして，糖鎖プロファイリング法によって糖鎖の変動を捉えることができるかどうかを検証した．

$5\times10^6$ 個程度の CHO 細胞と GnT-III 遺伝子導入 CHO 細胞を界面活性剤処理し，膜画分及び可溶性画分に分画した．それぞれの画分から PNGase F によって糖鎖を切り出し，$NaBH_4$ で還元後，LC/MS によるプロファイリングを行った．Fig. 3A は CHO 細胞の膜画分の糖鎖プロファイルである．各ピークのマススペクトルから，CHO 細胞の膜タンパク質に付加している糖鎖は高マンノース型糖鎖とシアル酸が結合した複合型 2 本鎖糖鎖が中心で，さらに混成型，トリマンノシルコア部分のみの糖鎖や，1 本鎖糖鎖などの比較的小さな糖鎖も結合していることが確認された．

Fig. 3B は，GnT-III 遺伝子導入細胞の膜画分の糖鎖プロファイルで，矢印で示す位置に CHO 細胞からは検出されない新たなイオンが検出された．GCC で糖鎖を分離した場合，bisecting GlcNAc が付加した糖鎖は付加されていない糖鎖より早く溶出される傾向がある．GnT-III 遺伝子導入によって新たに出現した糖鎖の分子量は，その後に溶出された 2 本鎖糖鎖の分子量より *N*-アセチルヘキソサミン (HexNAc) 1 分子分増加していることから，bisecting GlcNAc を有する 2 本鎖糖鎖であることが示唆された．

同様に可溶性画分についても糖鎖プロファイリングを行ったところ，膜画分とは異なるパターンが得られ，マススペクトルから，可溶性タンパク質に結合している糖鎖は主に高マンノース型であることがわかった．また，膜ほどではないが，GnT-III 遺伝子導入細胞の可溶性画分からも bisecting GlcNAc が付加していると思われる糖鎖が検出された．

Fig. 4 は CHO 細胞，及び GnT-III 遺伝子導入 CHO 細胞から切り出された主な糖鎖のピーク面積をアシアロ 2 本鎖糖鎖のピーク面積を 1.0 として相対的に表したもので，糖鎖分布の変化を示している．このグラフから，GnT-III の発現によって bisecting GlcNAc が付加したと思われる糖鎖は出現するものの，糖鎖全体の分布に大きな変化は生じていないことがわかる．これは，GnT-III 発現によって糖鎖構造に変化が生じたタンパク質が全体の一部であることを示唆していると考えられる．このように，GCC-LC/MS を用いた糖鎖プロファイリングは糖鎖の構造や分布の違いを簡単に識別できることから，健常及び病態サンプル間の糖鎖の差異解析法として有用であると思われる．

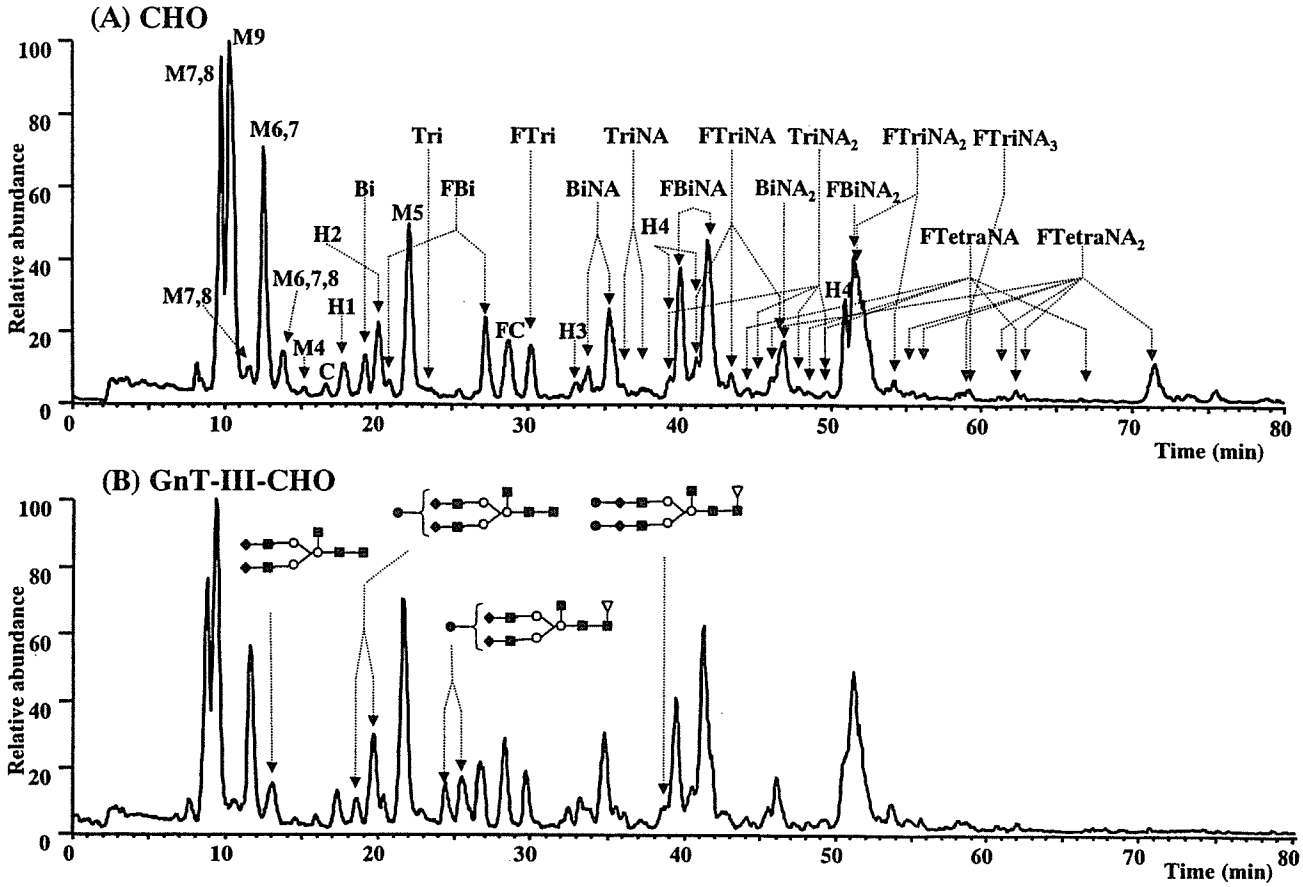


Fig. 3.　(A) CHO 細胞膜画分の糖鎖プロファイル，(B) GnT-III 遺伝子導入 CHO 細胞の糖鎖プロファイル

M, Man; H, hybrid; C, trimannosylcore; F, Fuc; NA, NeuAc; Bi, biantennary; Tri, triantennary; Tetra, tetraantennary

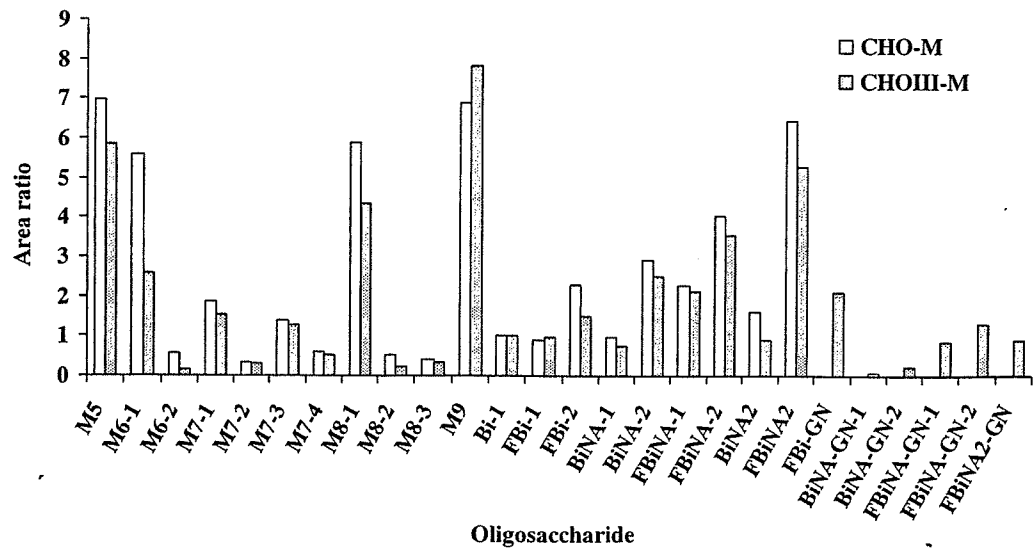


Fig. 4.　CHO 細胞膜画分 (CHO-M) 及び GnT-III 遺伝子導入細胞由来膜画分 (CHOIII-M) 由来糖鎖の分布

アシアロ 2 本鎖糖鎖を 1.0 とする

## 2. 糖タンパク質の同定と特性解析

糖鎖差異解析によって疾患関連糖鎖を見出すことができれば，プロテオミクスの手法を用いて，その糖鎖が付加しているタンパク質の同定と特性解析を行うことになる．可溶性タンパク質であれば，レクチンカラムや免疫沈降法などで得られた画分を SDS-PAGE 等で展開して目的糖タンパク質を得ることができるが，不溶性膜タンパク質の場合，レクチン等による分画が難しいケースが多く，2-DE 後，レ

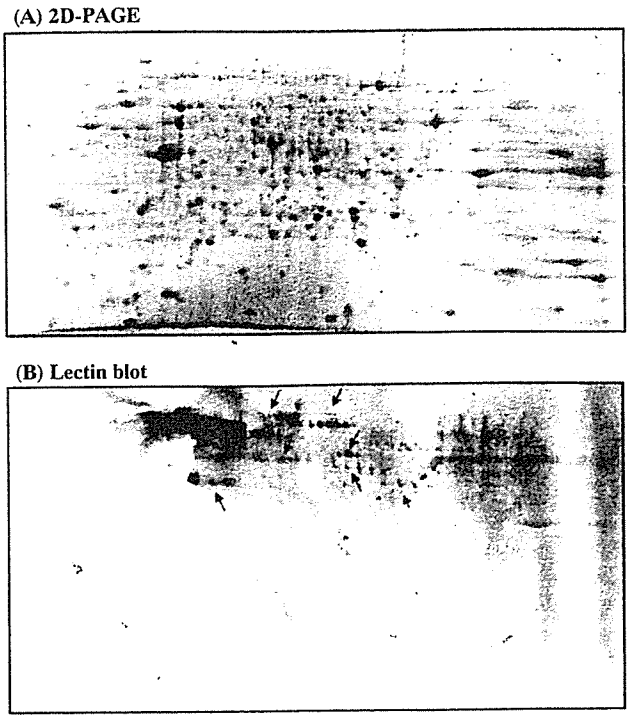


Fig. 5. GnT-III 遺伝子導入細胞膜画分の 2-DE

(A) Sypro Orange 染色, (B) PHA-$E_4$ ブロット
IEF, pH 3–10, 18 cm, 33,500 Vhr; SDS-PAGE, 12.5% gel (24×11 cm), 20 mA-0.5 hr, 50 mA-1.2 hr

クチンブロットなどにより糖タンパク質の位置を特定することになる[12]. しかし後者の場合, 泳動ゲルとレクチンブロット膜のマッチング, 及び特定されたゲル上タンパク質に目的糖鎖が付加していることの検証が必要となってくる.

Fig. 5 は, GnT-III 遺伝子導入細胞の膜画分を 2 枚のゲルで展開し, Sypro Orange で全タンパク質を染色した結果 (A), 及び bisecting GlcNAc を認識する PHA-$E_4$ レクチンを用いてレクチンブロットを行った結果 (B) を示している. レクチンブロットによって, 酸性側の 70–80 kDa 周辺に, 糖タンパク質に特徴的な train 状のスポットが複数組検出され, 一部のタンパク質の糖鎖に bisecting GlcNAc が付加されていることが確認された. 我々は, レクチンブロット上のスポットの位置から特定された泳動ゲル上の糖タンパク質の糖鎖の解析にも糖鎖プロファイリングが役立つと考えている. 現在, bisecting GlcNAc が付加していると推定されたスポットについて, ゲル内トリプシン消化に先立ち PNGase F 消化を行って糖鎖を切り出し, GCC-LC/MS を用いた bisecting GlcNAc の有無の確認と糖鎖構造解析を行っているところである.

## おわりに

GCC-LC/MS を用いた糖鎖プロファイリングは, 糖タンパク質性医薬品の特性・品質解析を目的として開発されたものである. この糖鎖プロファイリングが, 2-DE 等のプロテオミクス的手法と組み合わせることによって, 医薬品開発型研究のグライコミクスにも応用できる可能がでてきた. 電気泳動ゲル上の全タンパク質の中から糖タンパク質を検出する方法は報告されているが[13,14], 特定の糖鎖を付加している糖タンパク質のみを検出・抽出する方法は確立されておらず, それらを効率的に検出する方法の確立が今後の課題であろう.

## 文　献

1) Durand G, Seta N. Protein glycosylation and diseases: blood and urinary oligosaccharides as markers for diagnosis and therapeutic monitoring. Clin Chem 2000;46:795–805.
2) Fenselau C. MALDI MS and strategies for protein analysis. Anal Chem 1997;69:661A–665A.
3) Kawasaki N, Ohta M, Hyuga S, Hashimoto O, Hayakawa T. Analysis of carbohydrate heterogeneity in a glycoprotein using liquid chromatography/mass spectrometry and liquid chromatography with tandem mass spectrometry. Anal Biochem 1999;269:297–303.
4) Itoh S, Kawasaki N, Ohta M, Hyuga M, Hyuga S, Hayakawa T. Simultaneous microanalysis of N-linked oligosaccharides in a glycoprotein using microbore graphitized carbon column liquid chromatography/mass spectrometry. J Chromatogr 2002;168:89–100.
5) Kawasaki N, Itoh S, Ohta M, Hayakawa T. Microanalysis of N-linked oligosaccharides in a glycoprotein by capillary liquid chromatography/mass spectrometry and liquid chromatography/tandem mass spectrometry. Anal Biochem 2003;316:15–22.
6) Baker KN, Rendall MH, Hills AE, Hoare, M, Freedman RB, James DC. Metabolic control of recombinant protein N-glycan processing in NS0 and CHO cells. Biotechnol Bioeng 2001;73:188–202.
7) Sheeley DM, Merrill BM, Taylor LC. Characterization of monoclonal antibody glycosylation: comparison of expression systems and identification of terminal alpha-linked galactose. Anal Biochem 1997;247:102–110.
8) Rudd PM, Colominas C, Royle L, Murphy N, Hart E, Merry, AH, Hebestreit HF, Dwek RA. A high-performance liquid chromatography based strategy for rapid, sensitive sequencing of N-linked oligosaccharide modifications to proteins in sodium dodecyl sulphate polyacrylamide electrophoresis gel bands. Proteomics 2001;1:285–294.
9) Sheng Y, Yoshimura M, Inoue S, Oritani K, Nishiura T, Yoshida H, Ogawa M, Okajima Y, Matsuzawa Y, Taniguchi N. Remodeling of glycoconjugates on CD44 enhances cell adhesion to hyaluronate, tumor growth and metastasis in B16 melanoma cells expressing beta1,4-N-acetylglucosaminyltransferase III. Int J Cancer 1997;73:850–858.
10) Yoshimura M, Nishikawa A, Ihara Y, Taniguchi S, Taniguchi N. Suppression of lung metastasis of B16 mouse melanoma by N-acetylglucosaminyltransferase III gene transfection. Proc Natl Acad Sci USA 1995;92:8754–8758.

11) Yoshimura M, Ihara Y, Matsuzawa Y, Taniguchi N. Aberrant glycosylation of E-cadherin enhances cell-cell binding to suppress metastasis. J Biol Chem 1996;271:13811–13815.
12) Ekuni A, Miyoshi E, Ko JH, Noda K, Kitada T, Ihara S, Endo T, Hino A, Honke K, Taniguchi N. A glycomic approach to hepatic tumors in N-acetylglucosaminyltransferase III (GnT-III) transgenic mice induced by diethylnitrosamine (DEN): identification of haptoglobin as a target molecule of GnT-III. Free Radic Res 2002;36:827–833.
13) Wilson NL, Schulz BL, Karlsson NG, Packer NH. Sequential analysis of N- and O-linked glycosylation of 2D-PAGE separated glycoproteins. J Proteome Res 2002;1:521–529.
14) Schulenberg B, Beechem JM, Patton WF. Mapping glycosylation changes related to cancer using the Multiplexed Proteomics technology: a protein differential display approach. J Chromatogr B Analyt Technol Biomed Life Sci 2003;793:127–139.

Available online at www.sciencedirect.com
SCIENCE DIRECT®
Biologicals 32 (2004) 70–77
BIOLOGICALS
www.elsevier.com/locate/biologicals

# Analysis of site-specific glycosylation in recombinant human follistatin expressed in Chinese hamster ovary cells

Masashi Hyuga*, Satsuki Itoh, Nana Kawasaki, Miyako Ohta, Akiko Ishii, Sumiko Hyuga, Takao Hayakawa

*Division of Biological Chemistry and Biologicals, National Institute of Health Sciences, 1-18-1, Kamiyoga, Setagaya-ku, Tokyo 158-8501, Japan*

Received 22 October 2003; accepted 1 April 2004

**Abstract**

Follistatin (FS), a glycoprotein, plays an important role in cell growth and differentiation through the neutralization of the biological activities of activins. In this study, we analyzed the glycosylation of recombinant human FS (rhFS) produced in Chinese hamster ovary cells. The results of SDS-PAGE and MALDI-TOF MS revealed the presence of both non-glycosylated and glycosylated forms. FS contains two potential *N*-glycosylation sites, Asn95 and Asn259. Using mass spectrometric peptide/glycopeptide mapping and precursor-ion scanning, we found that both *N*-glycosylation sites were partially glycosylated. Monosaccharide composition analyses suggested the linkages of fucosylated bi- and triantennary complex-type oligosaccharides on rhFS. This finding was supported by mass spectrometric oligosaccharide profiling, in which the *m/z* values and elution times of some of the oligosaccharides from rhFS were in good agreement with those of standard oligosaccharides. Site-specific glycosylation was deduced on the basis of the mass spectra of the glycopeptides. It was suggested that biantennary oligosaccharides are major oligosaccharides located at both Asn95 and Asn259, whereas the triantennary structures are present mainly at Asn95.


*Abbreviations:* CHO, Chinese hamster ovary; FCS, fetal calf serum; FS, follistatin; GCC, graphitized carbon column; GnT, *N*-acetylglucosaminyltransferase; HPAEC-PAD, high-pH anion-exchange chromatography with pulsed amperometric detection; IEF, isoelectric focusing; LC/MS, liquid chromatography/mass spectrometry; MALDI-TOF MS, matrix-assisted laser desorption/ionization time-of-flight mass spectrometry; NeuAc, *N*-acetyl neuraminic acid; NeuGc, *N*-glucoryl neuraminic acid; PNGaseF, peptide *N*-glycanase F; rhFS, recombinant human follistatin; SDS-PAGE, sodium dodecyl sulfate-polyacrylamide gel electrophoresis; TFA, trifluoroacetic acid

## 1. Introduction

Follistatin (FS), a glycoprotein, was first discovered in ovarian follicular fluid as an inhibitor of pituitary follicle-stimulating hormone secretion [1,2]. Subsequent studies have revealed that FS can bind to activins and neutralize their biological activities [3,4]. Activins are members of the transforming growth factor-β superfamily, and they play important roles in the regulation of cell growth and in the differentiation processes that lead to morphogenesis in early vertebrate development [5,6]. Since FS and activins are broadly distributed, they are not confined solely to tissues associated with reproduction [7].

FS is present in heterogeneous forms [8]. The FS gene consists of 315 amino acids, and it includes six exons (Fig. 1); alternative splicing can generate two isoforms, i.e. a 315-amino-acid protein (the full-length form, FS315) and a 288-amino-acid protein (the carboxy-truncated form, FS288) [9]. The activin-neutralizing activity of FS288 is higher than that of FS315 [10,11], which appears to correlate with their heparin/heparan sulfate proteoglycan-binding abilities [12]. The heterogeneity of FS is also due to diverse glycosylation. FS has two potential *N*-glycosylation sites (Asn95 and Asn259). Oligosaccharides are generally known to play important roles in defining the properties of glycoproteins such as their biological activity, immunogenicity,

* Corresponding author. Fax: +81-3-3700-9084.
*E-mail address:* mhyuga@nihs.go.jp (M. Hyuga).

1045-1056/04/$30.00 
doi:10.1016/j.biologicals.2004.04.001


Fig. 1. Amino acid sequence of rhFS. Predicted cleavage sites with Asp-N are indicated by |. The potential *N*-glycosylation sites are indicated by boxes.

pharmacokinetics, solubility, and protease resistance [13,14]. Glycosylation on FS is also likely to exert an effect on activin-neutralizing activity; however, neither structure of the N-linked oligosaccharides in FS, nor their physiological roles, have been clarified due to the limited availability of these oligosaccharides.

The aim of this study was to elucidate the glycosylation of FS. We previously developed an oligosaccharide profiling method using liquid chromatography/mass spectrometry (LC/MS) equipped with a graphitized carbon column (GCC) [15–22]. Recently, we demonstrated a procedure for facilitating the structural analysis of glycoproteins [16]. Carbohydrate profiles and site-specific glycosylations can be characterized by the GCC-LC/MS method, followed by mass spectrometric peptide/glycopeptide mapping. We used this method to demonstrate here the carbohydrate heterogeneity and the site-specific N-linked oligosaccharide structures in recombinant human FS288 (rhFS) produced in Chinese hamster ovary (CHO) cells, in which a sufficient amount of FS could be expressed.

## 2. Materials and methods

### 2.1. Materials

Human FS315 cDNA and recombinant human activin A were kindly provided by Dr. Yuzuru Eto (Ajinomoto Co., Inc., Kawasaki, Japan). CHO cells were obtained from the Japanese Cancer Research Resources Bank (Tokyo, Japan). Mammalian expression vector pcDNA3.1/Hygro was purchased from Invitrogen (Carlsbad, CA, USA). LipofectAMINE plus reagent, Ham's F12 medium, fetal calf serum (FCS) and hygromycin were purchased from Life Technologies Inc. (Rockville, MD, USA). Pellicon XL membrane and Immobilon-P membrane were purchased from Millipore Corp. (Bedford, MA, USA). Sulfated-cellulofine was purchased from Seikagaku Corp. (Tokyo, Japan). Neuraminidase was purchased from Nakalai Tesque (Kyoto, Japan). *N*-glycosidase F (PNGaseF) and endoproteinase Asp-N (Asp-N) were purchased from Boehringer Mannheim (Mannheim, Germany). All other chemicals were obtained from commercial sources and were of the highest purity available.

### 2.2. Establishment of a CHO cell line expressing rhFS

Complementary DNA encoding human FS288, was constructed from FS315 cDNA, and was cloned into pcDNA3.1/Hygro. This expression vector was transfected into CHO cells with LipofectAMINE plus reagent, according to the manufacturer's instructions. To screen the transformants, the transfectants were cultured with Ham's F12 medium supplemented with 10% FCS and 1 mg/ml hygromycin. After 2 weeks, the colonies were lifted with a micropipette. Expression levels of rhFS were assessed by an activin-neutralizing assay. The candidates were cloned by limiting dilution twice and were assessed again. The most productive rhFS-expressing clone (CHO-FS) was used in the following experiments.

### 2.3. Preparation of rhFS

Semi-confluent CHO-FS cells were cultured in Ham's F12 medium supplemented with 2% FCS. The conditioned medium was concentrated to a 1/10 volume by filtration with a Pellicon XL membrane ($M_r$ 5000 cut), and was applied onto a sulfated-cellulofine column (2.5 × 20 cm) at 2 ml/min. The column was washed with 50 mM Tris–HCl (pH 8) containing 0.5 M NaCl, and the protein was eluted with 50 mM Tris–HCl (pH 8) containing 1.5 M NaCl. The effluent from the column was fractionated, and rhFS was monitored on Western blots using polyclonal anti-FS antibody. The fractions containing rhFS were injected into an HPLC (Hitachi D7000, Hitachi Co., Tokyo, Japan) apparatus equipped with a reversed-phase column (Vydac C4, 10 × 300 mm, The Separations Group, Inc., Hesperia, CA, USA). The protein was eluted with a linear gradient of 16–48% of acetonitrile/0.1% trifluoroacetic acid (TFA) for 30 min at a flow rate of 2 ml/min. Elution of proteins was monitored at 280 nm and individual peaks were manually collected. Fraction of rhFS was monitored on Western blots using polyclonal anti-FS antibody.

### 2.4. SDS-PAGE analysis of rhFS

RhFS was digested with or without PNGaseF at 37 °C for 24 h. The proteins were separated by sodium dodecyl sulfate-polyacrylamide gel electrophoresis

(SDS-PAGE) on 10% polyacrylamide gel. The gel was stained with Coomassie blue.

### 2.5. Isoelectric focusing

RhFS was dissolved in 100 mM ammonium acetate buffer, pH 4.5, and incubated with neuraminidase at 37 °C for 18 h. The proteins were precipitated with cold acetone and separated by isoelectric focusing (IEF). The gel was stained with Coomassie blue.

### 2.6. MALDI-TOF MS

RhFS (20 μg) was subjected to positive-ion matrix-assisted laser desorption/ionization time-of-flight mass spectrometry (MALDI-TOF MS), using a Shimazu/KRATOS MALDI I instrument (Shimazu Co., Kyoto, Japan) with 3,5-dimethoxy-4-hydroxy-cinnamic acid as the matrix.

### 2.7. Monosaccharide composition analysis

Monosaccharide composition analysis was performed according to the method reported by Hardy et al. [23]. Briefly, rhFS (50 μg) was hydrolyzed with 2 M TFA at 100 °C for 3 h. Monosaccharide compositions were analyzed by high-pH anion-exchange chromatography with pulsed amperometric detection (HPAEC-PAD) using a DX-300 system (Dionex, Sunnyvale, CA, USA) equipped with a CarboPac PA-1 anion exchange column (4 × 250 mm, Dionex).

### 2.8. Preparation of N-linked oligosaccharides alditols

N-linked oligosaccharides alditols were prepared by a previously described method [20]. Briefly, rhFS (100 μg) was digested with 5 units of PNGaseF at 37 °C for 2 days. Proteins were precipitated with 75% cold ethanol. The oligosaccharides were incubated with $NaBH_4$ at room temperature for 2 h. Excess reagent was decomposed with diluted acetic acid. The mixture was applied to a Supelclean ENVI-Carb column (Supelco, Bellefonte, PA, USA), which was washed with $H_2O$ to remove the salts. Borohydride-reduced oligosaccharides were eluted with 30% acetonitrile/5 mM ammonium acetate.

### 2.9. Sugar profiling by LC/MS

Sugar profiling was carried out using a MAGIC 2002 system (Michrom BioResources, Inc., Auburn, CA, USA) connected to a TSQ7000 triple-stage quadruple mass spectrometer (ThermoFinnigan, San Jose, CA, USA) in the positive-ion mode. The column used was a GCC (Hypercarb 5 μm, 1.0 × 150 mm, ThermoFinnigan). The eluents were 5 mM ammonium acetate (pH 9.6) containing 2% acetonitrile (pump A); and 5 mM ammonium acetate (pH 9.6) containing 80% acetonitrile (pump B). The N-linked oligosaccharide alditols were eluted at a flow rate of 50 μl/min for 80 min with a gradient of 5–30% in pump B. The ESI voltage was set at 4500 V, and the capillary temperature was 175 °C. The electron multiplier was set at 1200 V.

### 2.10. Asp-N digestion

RhFS was reduced and *S*-carboxymethylated as previously described [20]. Briefly, rhFS (100 μg) was dissolved in 0.5 M Tris–HCl buffer (pH 8.6) containing 8 M guanidine and 5 mM EDTA. After reduction with 2-mercaptoethanol at room temperature for 2 h, monoiodoacetic acid was added and incubated at room temperature for 2 h in the dark. Reduced and *S*-carboxymethylated-rhFS (equivalent to 100 μg of rhFS) was digested with Asp-N (2 μg) in 25 mM $NH_4HCO_3$ (pH 8.0) at 37 °C for 20 h. The predicted peptides to be obtained by Asp-N digestion were sequentially designated as D1–D15 (Fig. 1).

### 2.11. Peptide/glycopeptide mapping of Asp-N-digested rhFS

Peptide/glycopeptide mapping was carried out using a MAGIC 2002 system connected to a TSQ7000 triple-stage quadruple mass spectrometer in the positive-ion mode. The column used was a MAGIC C18 column (1.0 × 150 mm, Michrom BioResources). The eluents were 2% acetonitrile/0.05% TFA (pump A), and 80% acetonitrile/0.05% TFA (pump B). Asp-N-digested rhFS was eluted with a linear gradient from 5 to 45% in pump B at a flow rate of 50 μl/min for 40 min. The eluate was monitored at 206 nm. The ESI voltage was set at 4500 V, and the capillary temperature was 175 °C. The electron multiplier was set at 1200 V. Precursor-ion scanning was performed using argon gas as the collision gas at a pressure of 2 mTorr. The collision energy was adjusted to −25 eV. The scan rate was 3 s/scan.

## 3. Results

### 3.1. Heterogeneity of rhFS

The carbohydrate heterogeneity of rhFS was analyzed by SDS-PAGE with and without PNGaseF digestion. The intact rhFS migrated as bands of an apparent molecular mass of 32 kDa and 33–36 kDa under non-reducing conditions (Fig. 2A, lane 1). PNGaseF digestion resulted in the disappearance of the multiple bands at 33–36 kDa with increases in the 32-kDa band (Fig. 2A, lane 2). These results suggest that the 32 kDa band and higher molecular weight bands are

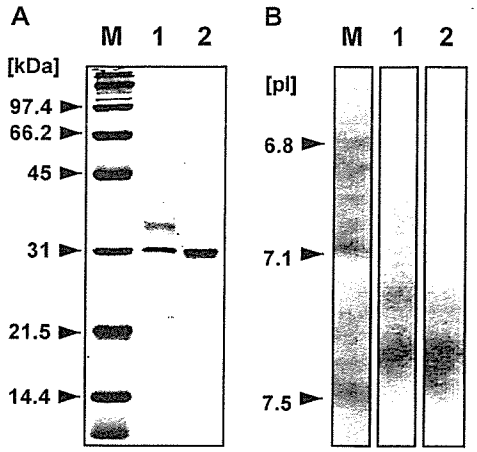


Fig. 2. (A) SDS-PAGE analysis of intact rhFS (lane 1) and PNGaseF-digested rhFS (lane 2). Lane M represents molecular weight markers. (B) IEF of intact rhFS (lane 1) and neuraminidase-digested rhFS (lane 2). Lane M represents p*I* markers.

the non-glycosylated FS and the glycosylated FS with diverse N-linked oligosaccharides, respectively.

The sialic acid heterogeneity of rhFS was analyzed by IEF with and without neuraminidase digestion. IEF of intact rhFS showed that the majority of the isoforms are located from p*I* 6.9 to 7.4 (Fig. 2B, lane 1). After treatment with neuraminidase, the acidic bands had disappeared and shifted at p*I* 7.4 (Fig. 2B, lane 2). These results suggested that the sialic acids contribute to the heterogeneity and the charge of rhFS.

The distribution of glycoforms was further investigated by MALDI-TOF MS. As shown in Fig. 3, multiple ions were detected in the range of 31.5–37 kDa. The most abundant ion at *m/z* 31,525 corresponded to the theoretical mass of non-glycosylated FS (31,514 Da). The other ions at *m/z* 33,804 and 35,600 could have been monoglycosylated FS and diglycosylated FS, respectively.

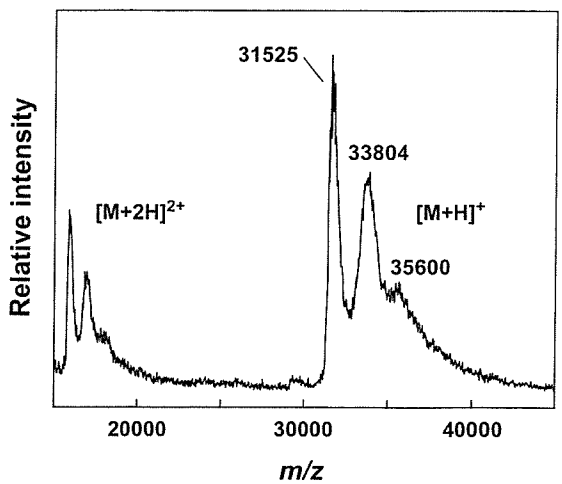


Fig. 3. MALDI-TOF MS analysis of intact rhFS. The peaks at *m/z* 31,525, 33,804 and 35,600 correspond to the non-glycosylated and glycosylated form of rhFS, respectively.

### 3.2. Monosaccharide composition of rhFS

Monosaccharide composition was analyzed by hydrolysis followed by HPAEC-PAD. The relative molecular ratio of fucose and glucosamine were estimated at 1.2 and 4.4, respectively, when mannose was considered as 3.0 (Table 1). This result suggests the presence of fucosylated bi- and triantennary-type oligosaccharides. No galactosamine residue was detected, suggesting the absence of O-linked oligosaccharides.

### 3.3. N-linked oligosaccharides in rhFS

N-linked oligosaccharides were released from rhFS by PNGaseF digestion and reduced with $NaBH_4$ to avoid the separation of anomers. Then the oligosaccharide alditols from rhFS were analyzed by GCC-LC/MS. Fig. 4 shows the total ion current chromatogram of N-linked oligosaccharide alditols. The *m/z* values of intense ions observed in major peaks (peaks 8 and 12) were $1040.7^{2+}$ and $1186.4^{2+}$, which were consistent with the theoretical *m/z* values of $[dHex][Hex]_5[HexNAc]_4[NeuAc]^{2+}$ and $[dHex][Hex]_5[HexNAc]_4[NeuAc]_2{}^{2+}$, respectively (Table 2). The elution times of these oligosaccharides were in good agreement with those of fucosyl biantennary oligosaccharides bearing mono- and di-NeuAc prepared from erythropoietin, respectively [24]. An ion at *m/z* $1041.4^{2+}$ was also detected in peak 6. This oligosaccharide could be a sialylation isomer of peak 8 ($1040.7^{2+}$).

Likewise, the ions at *m/z* $1790.7^{+}$ and $895.4^{2+}$ in peak 2 and at *m/z* $1077.9^{2+}$ in peak 3 were assigned as an asialo fucosylated biantennary oligosaccharide and an asialo fucosylated triantennary oligosaccharide, respectively. The ion at *m/z* $2389.6^{+}$ and $1194.6^{2+}$ in peak 11 was consistent with $[dHex][Hex]_5[HexNAc]_4[NeuAc][NeuGc]^{2+}$ or $[Hex]_6[HexNAc]_4[NeuAc]_2{}^{2+}$, respectively. The ions at *m/z* $2097.7^{+}$ and $1048.6^{2+}$ in peak 5 and at *m/z* $2096.5^{+}$ and $1049.5^{2+}$ in peak 8 were consistent with $[dHex][Hex]_5[HexNAc]_4[NeuGc]^{2+}$ or $[Hex]_6[HexNAc]_4[NeuAc]^{2+}$, respectively. The minor ions at *m/z* $1224.1^{2+}$, $1224.3^{2+}$, $1369.7^{2+}$, $1369.8^{2+}$,

Table 1
Monosaccharide composition analysis of rhFS oligosaccharides

| Monosaccharide | Relative molar proportions[a] |
|---|---|
| Fucose | 1.2 |
| Galactosamine | 0.3 |
| Glucosamine | 4.4 |
| Galactose | 3.2 |
| Glucose | 0.3 |
| Mannose | 3.0 |

[a] Data are normalized to three-mannose residues.

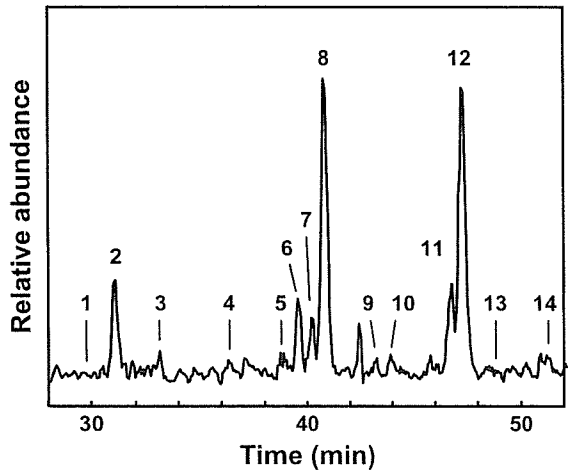


Fig. 4. Sugar map of oligosaccharide alditols released from rhFS. N-linked oligosaccharide alditols from rhFS were separated with GCC. The total ion content was scanned using the positive-ion mode at $m/z$ 700–2400.

$1370.5^{2+}$ and $1515.5^{2+}$ in peaks 7, 9, 11, 12, 13 and 14 were deduced to the fucosylated triantennary oligosaccharides with NeuAc, respectively.

The ratio of oligosaccharides was estimated as follows: fucosylated biantennary, ca. 85%, and fucosylated triantennary structures, ca. 10%, based on their ion currents; these results were in good agreement with the results of the monosaccharide composition analysis.

### 3.4. Site-specific glycosylation of rhFS

FS contains two potential *N*-glycosylation sites (Asn95 and Asn259, Fig. 1). The site-specific glycosylation and other post-translational modifications, such as phosphorylation and hydroxylation, were analyzed by mass spectrometric peptide/glycopeptide mapping (Fig. 5a, Table 3). Most of the non-glycosylated peptides were detected except for the small peptides, i.e. peptides D2 (tripeptide), D13 (tetrapeptide), and D12 (pentapeptide), which suggests the absence of *O*-glycans and any post-translational modifications on these peptides. The small peptides have no putative *N*-glycosylation site (Fig. 1), and no galactosamine residue was detected (Table 1). These findings suggest the absence of N- and O-linked oligosaccharides. However, the possibility remains that the small peptides are modified, such as by phosphorylation. Two unpredicted peptides ($m/z$ $1176.2^{2+}$ and $510.4^{2+}$) were detected among the Asp-N digests of rhFS. They were assigned to peptides D15-1 and D15-2, which were produced from peptide D15 by further cleavage at the amino-terminal of Glu280. It was reported that a cleavage at the N-terminal site of glutamic acid is a possible cut site for Asp-N under the same conditions [25]. Peptides D5 and D15-1, each of which have potential glycosylation site, were detected as non-glycosylated forms in the peptide/glycopeptide map.

Precursor-ion scanning, which can detect [Hex][HexNAc]$^+$ at $m/z$ 366 produced by collision-induced dissociation, was performed for the monitoring of the glycopeptides. The TIC chromatogram of the precursor-ion scanning showed two significant peaks, peaks G1 and G2 (Fig. 5b). Fig. 6 shows the mass spectra of peaks G1 and G2 in Fig. 5b. On the basis of the theoretical masses of the peptides and oligosaccharides identified by sugar mapping (Table 2), peaks G1 and G2

Table 2
Putative structures of N-linked oligosaccharides deduced from the GCC-LC/MS

| Peak No.[a] | Carbohydrate structure[b] | Theoretical mass[c] | Observed mass[d] | | |
|---|---|---|---|---|---|
| | | | $M^+$ | $M^{2+}$ | $M^{3+}$ |
| 1 | 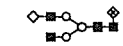 | 1627.5 | 1628.3 | 814.2 | - |
| 2 | 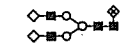 | 1789.7 | 1790.7 | 895.4 | - |
| 3 | 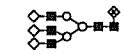 | 2155.0 | - | 1077.9 | - |
| 4 | 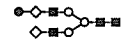 | 1934.7 | - | 967.9 | - |
| 5 | 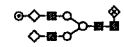 *1 | 2096.9 | 2097.7 | 1048.6 | - |
| 6 | 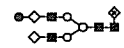 | 2080.9 | 2081.2 | 1041.4 | - |
| 7 | 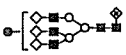 | 2446.3 | - | 1224.1 | 817.4 |
| 8 | 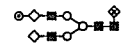 *1 | 2096.9 | 2096.5 | 1049.6 | - |
| | 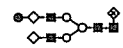 | 2080.9 | 2082.2 | 1040.7 | - |
| 9 | 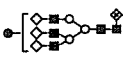 | 2446.3 | - | 1224.3 | - |
| 10 | 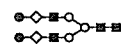 | 2226.0 | - | 1114.2 | - |
| 11 | 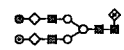 *2 | 2388.2 | 2389.6 | 1194.6 | - |
| |  | 2737.5 | - | 1369.7 | 913.4 |
| 12 | 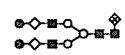 | 2372.2 | 2372.2 | 1186.4 | - |
| | 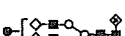 | 2737.5 | - | 1369.8 | - |
| 13 | 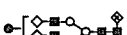 | 2737.5 | - | 1370.5 | 913.8 |
| 14 | 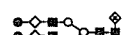 | 3028.8 | - | 1515.5 | - |

Note: The observed $m/z$ of *1 and *2 are also consistent with the theoretical $m/z$ value of $[Hex]_6[HexNAc]_4[NeuAc]$ and $[Hex]_6[HexNAc]_4[NeuAc]_2$, respectively.

[a] Peak label in Fig. 4.

[b] Proposed structures based on molecular weight. Symbols: solid squares, GlcNAc; open circles, mannose; open diamonds, galactose; dotted diamonds, fucose; solid circle, NeuAc; dotted circle, NeuGc.

[c] Calculated average mass.

[d] Mass of the ion measured in the positive-ion ESI mass spectrum from alditols.

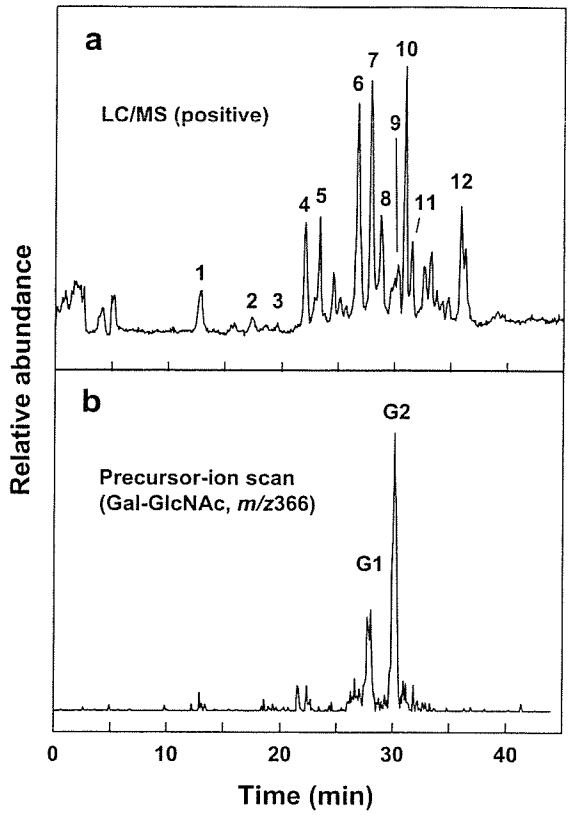


Fig. 5. Peptide/glycopeptide map of the rhFS Asp-N digest. The total ion current chromatogram of LC/MS in the positive-ion mode at $m/z$ 400–2400 (a), and the TIC chromatogram of LC/MS/MS, precursor-ion scan of $m/z$ 366 (b).

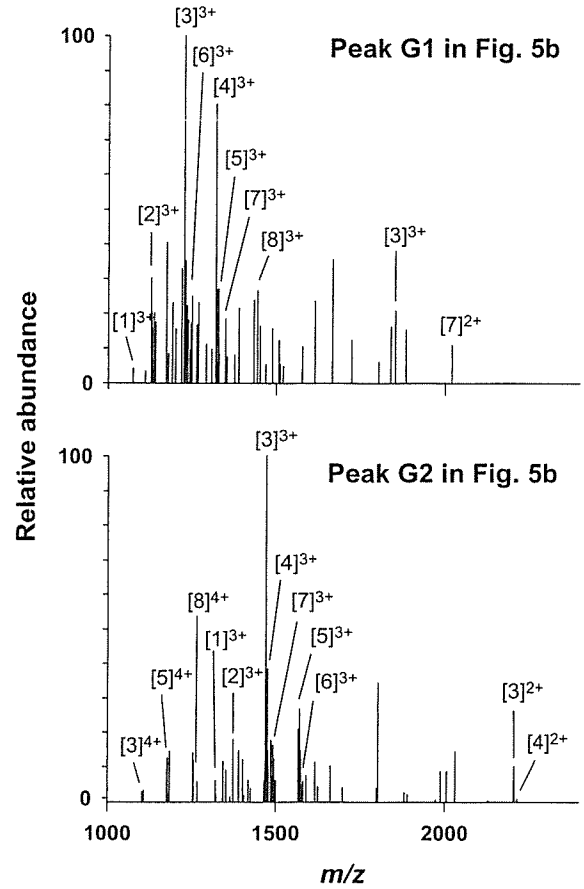


Fig. 6. Mass spectra of glycopeptides in peaks G1 and G2 in Fig. 5b. The observed $m/z$ value of each ion is summarized in Table 4.

were assigned to glycosylated D5 and D15-1, respectively. The oligosaccharides attached to each *N*-glycosylation site were deduced as shown in Table 4. By comparing the N-linked oligosaccharide structures on Asn95 with those on Asn259, it was concluded that biantennary oligosaccharides are major oligosaccharides located at both Asn95 and Asn259, whereas the triantennary structures are present mainly at Asn95.

Table 3
Assignment of the peaks in Fig. 5a

| Peak no.[a] | Peptide[b] | Theoretical mass[c] | Observed $m/z$[d] | | | | | |
|---|---|---|---|---|---|---|---|---|
| | | | $M^{+}$ | $M^{2+}$ | $M^{3+}$ | $M^{4+}$ | $M^{5+}$ | $M^{6+}$ |
| 1 | D4 | 2666.0 | – | 1334.2 | 889.9 | 667.4 | – | – |
| 2 | D14 | 777.8 | 778.6 | – | – | – | – | – |
| 3 | D15-2[e] | 1018.0 | 1019.0 | 510.4 | – | – | – | – |
| 4 | D11 | 1456.6 | 1457.5 | 729.0 | 486.3 | – | – | – |
| 5 | D6 | 4378.8 | – | – | 1460.8 | 1095.5 | – | – |
| 6 | D8 | 3326.4 | – | 1664.6 | 1109.5 | – | – | – |
| | D10 | 1467.6 | 1468.2 | 734.8 | 490.1 | – | – | – |
| 7 | D1 | 4728.1 | – | – | 1577.0 | 1183.2 | 947.0 | 789.6 |
| 8 | D7 | 1329.4 | 1330.2 | 665.3 | – | – | – | – |
| 9 | D5 | 1608.7 | 1609.3 | 805.1 | – | – | – | – |
| 10 | D9 | 4165.6 | – | – | 1389.0 | 1042.2 | 834.1 | – |
| 11 | D15-1[e] | 2350.6 | – | 1176.2 | 784.2 | – | – | – |
| 12 | D3 | 3219.5 | – | 1610.1 | 1073.8 | 806.4 | – | – |

[a] Peak label in Fig. 5a.
[b] Predicted peptides were shown in Fig. 1.
[c] Calculated average mass.
[d] Mass of the ions measured in the positive-ion ESI mass spectrum from precursor-ion scan.
[e] Peptide derived from D15 peptide.

## 4. Discussion

The aim of the present study was to analyze the distribution of the glycoforms and the carbohydrate structures of rhFS. Previous study of FS isolated from porcine ovary has shown that porcine FS exists in six isoforms, due to alternative splicing and the site occupancy of N-linked oligosaccharides [8]. In this study, we used rhFS288 to eliminate the heterogeneity due to alternative splicing. The results of SDS-PAGE and MALDI-TOF MS revealed the presence of both non-glycosylated and glycosylated forms (Figs. 2 and 3). FS contains two potential *N*-glycosylation sites. Using mass spectrometric peptide/glycopeptide mapping and precursor-ion scanning, we found that both *N*-glycosylation sites were partially glycosylated (Fig. 5 and Table 3). Non-glycosylated and glycosylated proteins containing Asn95 and Asn259 were detected in the peptide/glycopeptide map and precursor-ion scanning, respectively. Monosaccharide composition analyses suggested the presence of linkages of fucosylated bi- and triantennary complex-type oligosaccharides on rhFS (Table 1). This finding was supported by mass spectrometric oligosaccharide profiling, in which the *m/z* values and elution times of some of the oligosaccharides from rhFS were in good agreement with those of standard oligosaccharides. The site-specific glycosylations were deduced on the basis of the mass spectra of glycopeptides. It was suggested that biantennary oligosaccharides attach to both Asn95 and Asn259, whereas triantennary oligosaccharides attach mainly to Asn95 (Fig. 6 and Table 4).

Asn95 is located in the follistatin domain I, which is thought to be the heparin-binding site [26]. The site occupancy and structure of N-linked oligosaccharides on Asn95 may affect the heparin-binding ability of FS. Heparin/heparan sulfate proteoglycans are known to exert an important influence on FS, which neutralizes the activity of activins. It is therefore possible that sialylated oligosaccharides at Asn95 control the activin-neutralizing activity via modulation of the heparin-binding ability of FS. In fact, it was reported that the *N*-glycosylation isoforms of antithrombin and heparin cofactor II differ substantially in their affinity for heparin [27,28]. We are currently studying the role played by oligosaccharides in the activin-neutralizing activity of FS; these studies employ the carbohydrate remodeling technique using the CHO cell line established in the present study.

Table 4
Putative structures of N-linked oligosaccharides deduced from the LC/MS of the glycopeptides corresponding to the Asn95 and Asn259

| Carbohydrate Structure[a] | Asn95 | | | | | Asn259 | | | | |
|---|---|---|---|---|---|---|---|---|---|---|
| | Ions in peak G1 | Theoretical mass[b] | Observed *m/z*[c] | | | Ions in peak G2 | Theoretical mass[b] | Observed *m/z* | | |
| | | | $M^{2+}$ | $M^{3+}$ | $M^{4+}$ | | | $M^{2+}$ | $M^{3+}$ | $M^{4+}$ |
| 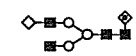 | 1 | 3216.2 | - | 1073.4 | - | 1 | 3958.1 | - | 1319.6 | - |
| 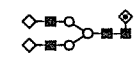 | 2 | 3378.6 | - | 1126.6 | - | 2 | 4120.5 | - | 1373.9 | - |
| 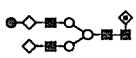 | 3 | 3669.6 | 1835.7 | 1223.2 | - | 3 | 4411.5 | 2206.3 | 1471.8 | 1104.7 |
| 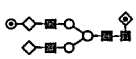 | - | | - | | - | 4 | 4427.5 | 2214.8 | 1475.7 | - |
| 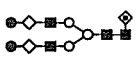 | 4 | 3960.9 | - | 1320.6 | - | 5 | 4702.8 | - | 1569.5 | 1177.1 |
| 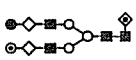 | 5 | 3976.6 | - | 1326.8 | - | 6 | 4718.8 | - | 1574.5 | - |
| 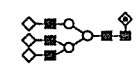 | 6 | 3743.7 | - | 1248.6 | - | 7 | 4485.6 | - | 1497.2 | - |
| 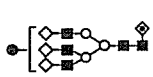 | 7 | 4034.9 | 2017.5 | 1346.9 | - | - | - | - | - | - |
| 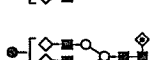 | 8 | 4326.2 | - | 1444.1 | - | 8 | 5068.1 | - | - | 1267.6 |

[a] Proposed structures based on molecular weight. Symbols: solid squares, GlcNAc; open circles, mannose; open diamonds, galactose; dotted diamonds, fucose; solid circle, NeuAc; dotted circle, NeuGc.

[b] Calculated average mass.

[c] Mass of the ion measured in the positive-ion ESI mass spectrum from precursor-ion scan. Mass spectra were shown in Fig. 6.